

รายงานวิจัยฉบับสมบูรณ์

การสังเคราะห์วัสดุเรื่องแสงที่มีโครงสร้างนาในที่อุณหภูมิต่ำ เพื่อใช้ในภาคอุตสาหกรรม

Synthesis of Luminescent Nano-structured Materials at Low Temperature for Using in Industrial Sectors

โดย รองศาสตราจารย์ ธิติพันธุ์ ทองเต็ม และคณะ

เมษายน 2554

รายงานวิจัยฉบับสมบูรณ์

การสังเคราะห์วัสดุเรื่องแสงที่มีโครงสร้างนาในที่อุณหภูมิต่ำ เพื่อใช้ในภาคอุตสาหกรรม

Synthesis of Luminescent Nano-structured Materials at Low Temperature for Using in Industrial Sectors

คณะผู้วิจัย

รองศาสตราจารย์ ธิติพันธุ์ ทองเต็ม มหาวิทยาลัยเชียงใหม่ ศาสตราจารย์ ดร. สมชาย ทองเต็ม มหาวิทยาลัยเชียงใหม่ อาจารย์วัลย์ชัย พรมในภาศ มหาวิทยาลัยเชียงใหม่

สนับสนุนโดยสำนักงานกองทุนสนับสนุนการวิจัย

กิตติกรรมประกาศ

คณะผู้วิจัยฯ ขอขอบคุณ สำนักงานกองทุนสนับสนุนการวิจัย (ส.ก.ว.) กรุงเทพ 10400 ที่ได้สนับสนุน ทุนวิจัยพื้นฐาน แบบมุ่งเป้า "นาในศาสตร์ และนาในเทคในโลยี "เป็นระยะเวลา 3 ปี

พร้อมกันนี้คณะผู้วิจัยขอขอบคุณ คณะวิทยาศาสตร์ มหาวิทยาลัยเชียงใหม่ ที่ให้ใช้สถานที่และ อำนวยความสะดวกต่าง ๆในการทำวิจัย ทำให้งานวิจัยนี้สำเร็จลุล่วงไปได้ด้วยดี

Shiding notific

(รองศาสตราจารย์ ธิติพันธุ์ ทองเต็ม) หัวหน้าโครงการวิจัยฯ

บทคัดย่อ

ในงานวิจัยนี้ได้สังเคราะห์ผลึกที่มีขนาดนาโนและไมโครเมตรของ BaWO4, SrWO4, CaWO4, CuS, CdS และ PbS ที่มี morphologies ต่าง ๆ กัน ได้สำเร็จด้วยวิธีต่าง ๆ กันได้แก่ cyclic microwave radiation, sonochemical method, solvothermal-microwave process และ hydrothermal reaction จากการตรวจหา phases ต่าง ๆ และ phase transition โดย XRD และ SAED พบว่ามีความสอดคล้องกันเป็นอย่างดี และ สอดคล้องกับที่ได้จากการ simulations เช่นกัน จากการศึกษาทั้ง FTIR และ Raman ได้แสดงถึง vibration ของ อะตอมต่าง ๆ ใน products ทั้งชนิด stretching และ bending modes รวมทั้งจากการตรวจสอบด้วย SEM และ TEM พบว่าอนุภาคที่ได้มีขนาดอยู่ในระดับนาโนและไมโครเมตรและมี morphologies ต่าง ๆ กัน ขึ้นอยู่ กับสารตั้งต้นที่ใช้ สภาวะในการสังเคราะห์ วิธีการสังเคราะห์ ตลอดจนสารเติมแต่งที่เติมลงไปด้วย นอกจากนี้ ยังได้ตรวจพบ PL emissions ที่ wavelengths ต่าง ๆ กัน ซึ่งเกิดจากการ transitions ของ electrons ใน products ต่าง ๆ และมีความสอดคล้องกับในรายงานอื่น ๆ เป็นอย่างดี

Abstract

In the present research, nano- and micro-crystals of BaWO₄, SrWO₄, CaWO₄, CuS, CdS and PbS with different morphologies were successfully synthesized using cyclic microwave radiation, sonochemical method, solvothermal-microwave process, and hydrothermal reactions. Their phases and phase transition were detected by XRD and SAED, in good accordance among them, and their corresponding simulations. The FTIR and Raman studies revealed the presence of the stretching and bending modes of atoms, containing in the products. The SEM and TEM characterization presented nano and microparticles with different morphologies, controlled by the starting agents, synthesis conditions, methods, and additives. In addition, their PL emissions were detected at different wavelengths, due to the electronic transitions of the products - in good accordance with those of other reports.

สารบาญ

กิตติกรรมประกาศ	2
บทคัดย่อ	3
Abstract	4
บทน้ำ	6
Characterization of nano- and micro-crystalline CdS synthesized	7
using a cyclic microwave radiation	
Formation of CuS with flower-like, hollow spherical, and tubular structures	18
using the solvothermal-microwave process	
Influence of cetyltrimethylammonium bromide on the morphology of AWO ₄	35
(A = Ca, Sr) prepared by cyclic microwave irradiation	
Characterization of MeWO ₄ (Me = Ba, Sr and Ca) nanocrystallines prepared	44
by sonochemical method	
Characterization of PbS with different morphologies produced using a cyclic	55
microwave radiation	
Preparation of ear-like, hexapod and dendritic PbS using cyclic	66
microwave-assisted synthesis	
Carboxymethyl cellulose-assisted hydrothermal synthesis of PbS with nano	74
and microcrystals	
Output ที่ได้จากโครงการวิจัย ฯ	86
ผลงานวิจัยที่เผยแพร่ในวารสารต่าง ๆ	92

บทน้ำ

ปัจจุบัน วัสดุที่มีโครงสร้างในระดับนาโนและไมโครเมตร กำลังเป็นที่สนใจกันมากเนื่องจากมี ประโยชน์ในการนำไปประยุกต์ใช้ในอุตสาหกรรมต่าง ๆ ได้อย่างกว้างขวาง สำหรับในประเทศไทย ได้มีการ นำเข้าจากต่างประเทศทั้งในลักษณะที่เป็นวัตถุดิบและสำเร็จรูปเป็นจำนวนมาก ซัลไฟด์ ทั้งสเตท และโมลิบเดต จำนวนมาก เป็นสารที่มีสมบัติเรื่องแสงที่น่าสนใจทั้งในทางการค้า และอุตสาหกรรมเป็นอย่างมาก สามารถ นำไปประยุกต์ใช้ทางด้านที่เกี่ยวกับ flat panel display, luminescent device, infrared window, solar cell, lasers, microwave, optical fiber, catalyst ใช้ใน Raman scattering behavior และอื่น ๆ ในปัจจุบันนี้ได้มี การทำวิจัยกันอย่างกว้างขวางเพื่อสังเคราะห์สารดังกล่าวให้มีรูปร่างต่าง ๆ กัน ซึ่งจะทำให้สารมีสมบัติที่ แตกต่างกันด้วย ทั้งนี้ขึ้นอยู่กับกระบวนการและสภาวะที่ใช้สังเคราะห์ และอื่น ๆ

สำหรับการวิจัยนี้ได้สังเคราะห์ ผลึกที่มีขนาดนาโนเมตรและไมโครเมตรของ $BaWO_4$, $SrWO_4$, $CaWO_4$, CuS, CdS และ PbS ที่มี morphologies ต่าง ๆ กันได้สำเร็จด้วยวิธีต่าง ๆ กันคือ cyclic microwave radiation, sonochemical method, solvothermal-microwave process และ hydrothermal reaction จากนั้น ได้ตรวจสอบหา phases และ phase transformation, morphologies, vibrational modes ตลอดจน สมบัติการเรื่องแสงและอื่น ๆ โดยมีรายละเอียดดังต่อไปนี้

Characterization of nano- and micro-crystalline CdS synthesized using a cyclic microwave radiation

Abstract

Nano- and micro-crystalline CdS was synthesized from cadmium [CdCl₂.2H₂O, Cd(NO₃)₂.4H₂O, Cd(CH₃COO)₂.2H₂O] and sulfur [CH₃CSNH₂, CH₅N₃S, CH₆N₄S] sources in ethylene glycol assisted by a cyclic microwave radiation at different conditions. Phases (hcp and cubic) and morphologies (rose-shaped particles, spikes in cluster, cauliflowers and nano-particles in cluster) were detected using XRD, SAED, TEM and SEM, and influenced by Cd and S sources. The crystalline products are aligned in systematic array analyzed by HRTEM. A Raman spectrometer revealed the presence of fundamental and overtone modes at 298 and 597 cm⁻¹, respectively. Exposure times and microwave powers also play a role in the crystallinity and size of the products.

Keywords: A. Cyclic microwave radiation, B. CdS (hcp and cubic), C. Rose-shaped particles, D. Spikes in cluster, E. Cauliflowers

CdS is one of the II-VI compounds having unique properties [1]. It has promising applications for light emitting diodes [2], solar cells [2], optoelectronics [3], catalysts [3] and others. There are different methods used to synthesize CdS such as solvothermal synthesis [2], hydrothermal process [3] and microwave irradiation [4]. Among the products with the same phase, different morphologies such as nanowires [2], nanorods [3], nanoparticles [4], flower-like particles [5], and hexagonal and triangular plates [6] were synthesized.

To synthesize CdS with different phases and morphologies, each of 0.005 mol cadmium [CdCl₂.2H₂O, Cd(NO₃)₂.4H₂O, Cd(CH₃COO)₂.2H₂O] and sulfur [CH₃CSNH₂, CH₅N₃S, CH₆N₄S] sources was dissolved in 30 ml ethylene glycol. Each mixture was stirred for 30 min and left for the reaction to proceed by a cyclic microwave radiation at different powers and exposure times. Each cycle was 100 s long, and composed of 30 and 70 s for the on and off periods, respectively. The precipitates were washed with water and ethanol, dried at 80 °C for 24 h and further analyzed.

XRD spectra (Figs 1 and 2) were compared with those of the JCPDS software (reference codes: 06-0314 and 80-0019) [7]. The products synthesized using CdCl₂.2H₂O and CH₃CSNH₂ at different exposure times and microwave powers (Fig. 1) were identified as CdS (hcp). The spectra are very sharp showing that the products compose of crystalline particles. The degree of crystallinity was increased with the increasing in the exposure time and microwave power. The effects of Cd and S sources on the phase were studied (Fig 2). The products synthesized using CdCl₂.2H₂O and one of the sulfur sources [CH₃CSNH₂, CH₅N₃S, CH₆N₄S] are CdS (hcp). Those synthesized using Cd(NO₃)₂.4H₂O or Cd(CH₃COO)₂.2H₂O and CH₃CSNH₂ are CdS (cubic). These show that Cd sources have the influence on the crystal structure. Two peaks at $2\theta = 36.65$ and 47.88 deg are the characteristics of hcp phase [8]. They diffracted from (102) and (103) planes of the products. Other two peaks diffracting from (002) and (110) planes of hcp phase are almost at the same Bragg's angles as those diffracting from (111) and (220) planes of cubic phase, respectively. Their planar spaces with the corresponding Bragg's angles are almost at the same values as well. XRD peaks of different structures are able to diffract from the same Bragg's angle, but the diffraction planes are different. Generally, CdS (hcp) is more thermodynamically stable than CdS (cubic) [9]. For the present research, no other characteristic peaks of impurity were detected showing that the products (Figs 1 and 2) are pure phase.

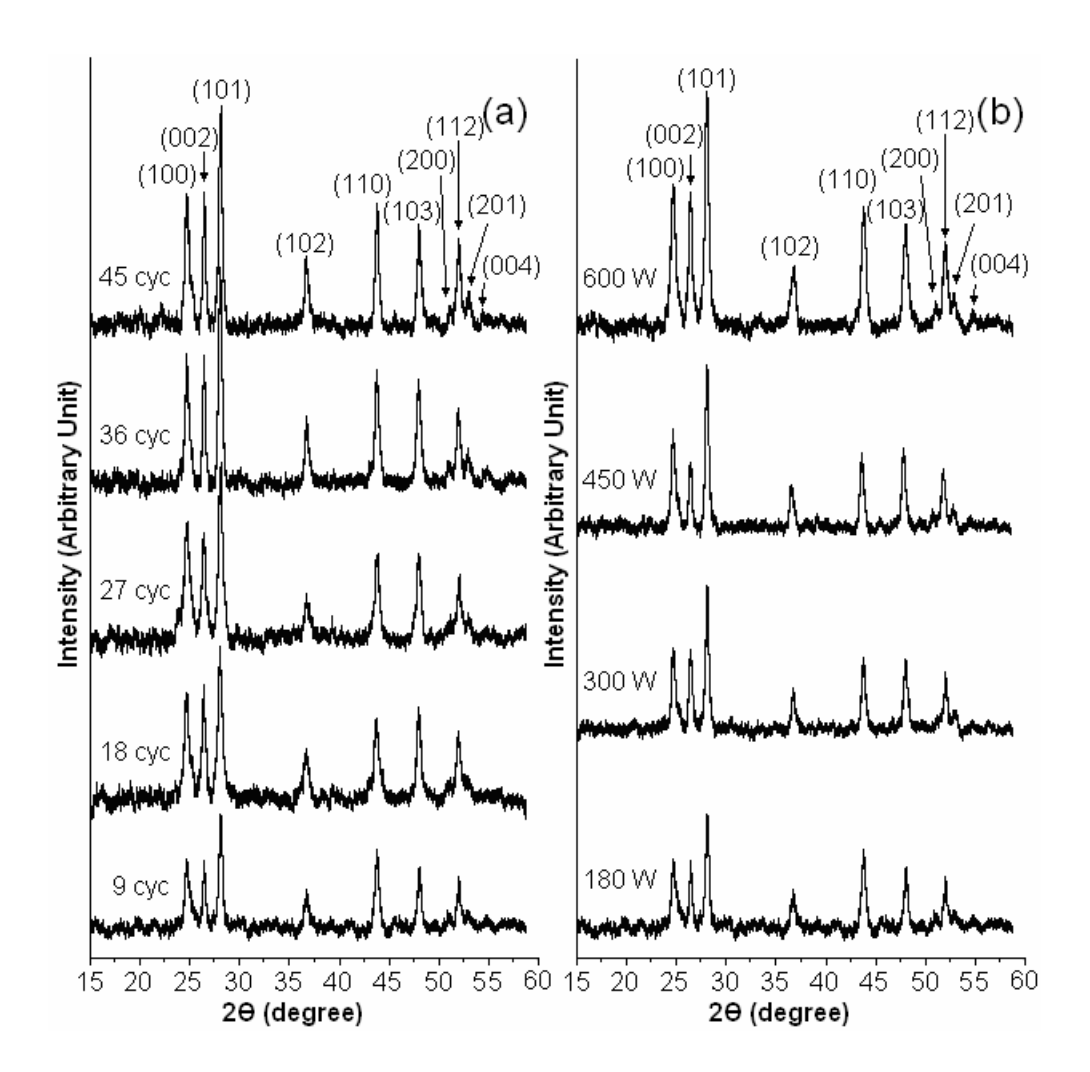


Fig 1. XRD spectra of the products prepared using CdCl₂.2H₂O and CH₃CSNH₂ at (a) 180 W for different cycles (cyc.), and (b) different microwave powers for 9 cycles.

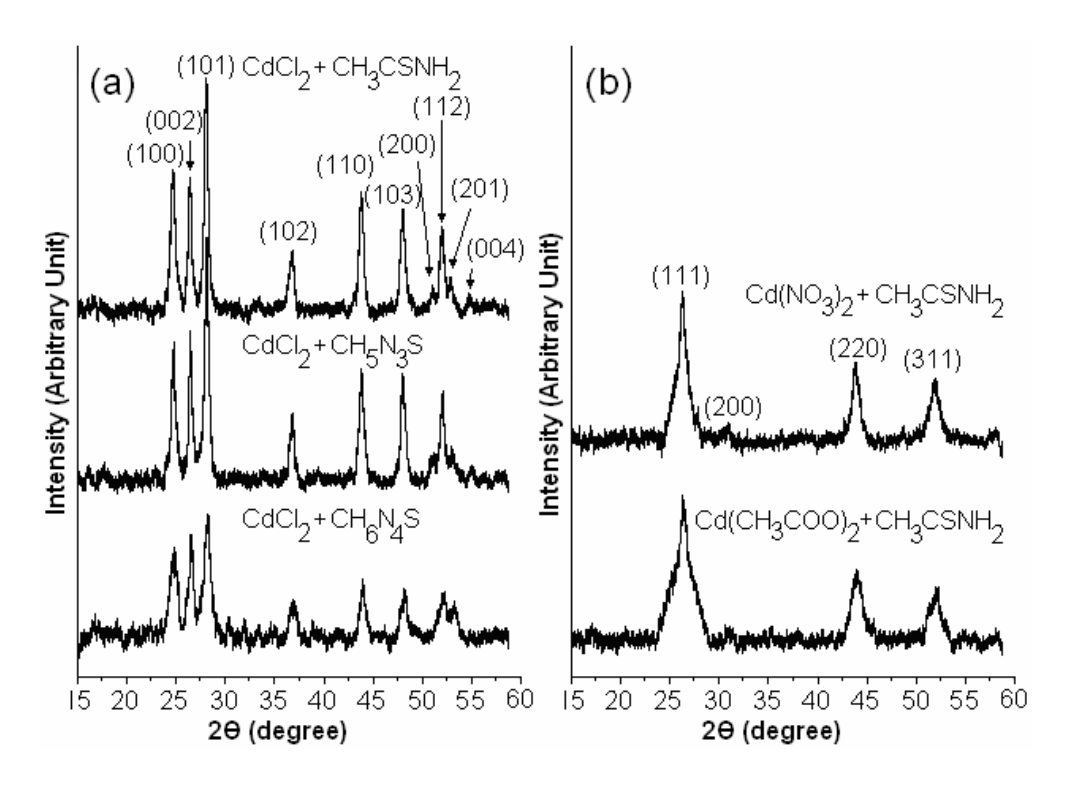


Fig 2. XRD spectra of the products prepared using different Cd and S sources at 600 W for 9 cycles. (a and b) are hcp and cubic phases, respectively.

Raman spectra (Fig 3) are almost identical to each other although the products have different phases (hcp and cubic). Two peaks were detected on both crystal structures. They are the first and second longitudinal optical (LO) phonon modes. The strong 1LO and weak 2LO correspond to the fundamental and overtone modes [10]. The vibrations of both phases, coinciding with each other [11], are at 298 and 597 cm⁻¹, respectively. Some defects can play role in the spectra as well.

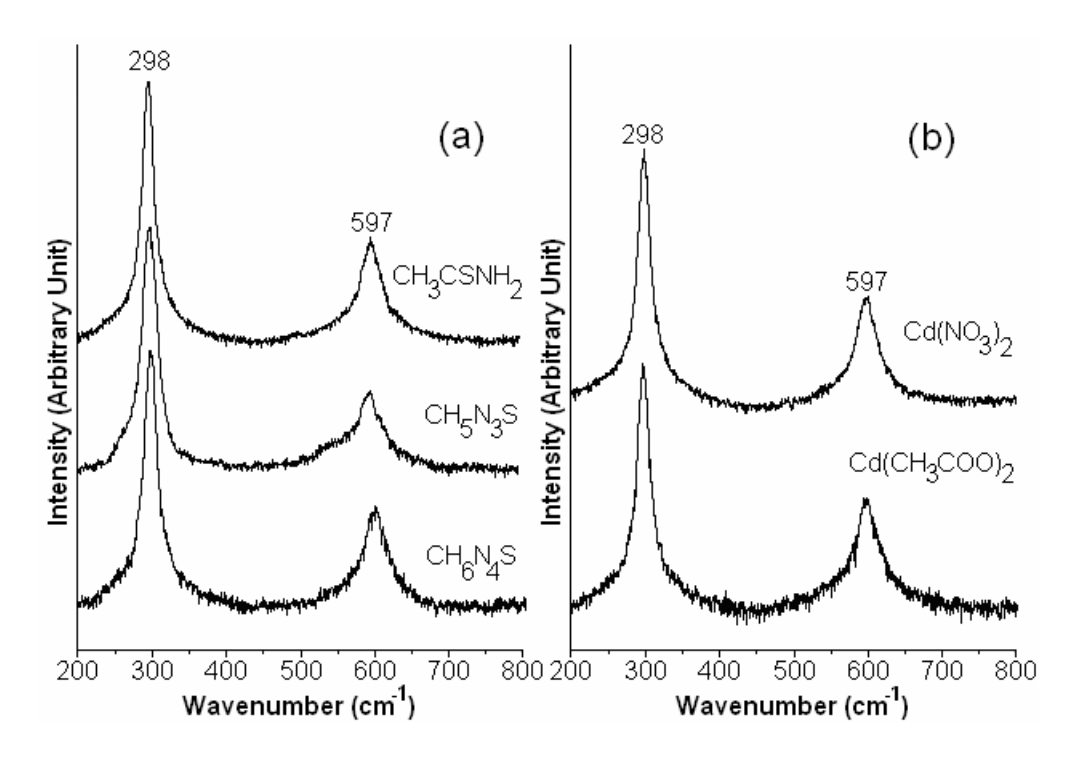


Fig 3. Raman spectra of the products prepared at 600 W for 9 cycles by using (a) CdCl₂.2H₂O and one of the S sources [CH₃CSNH₂, CH₅N₃S, CH₆N₄S], and (b) one of the Cd sources [Cd(NO₃)₂.4H₂O, Cd(CH₃COO)₂.2H₂O] and CH₃CSNH₂.

SEM images (Fig 4) show that the product morphologies are in the shapes of roses, spikes in cluster and cauliflowers for respective using CH₃CSNH₂, CH₅N₃S and CH₆N₄S as S sources, and CdCl₂.2H₂O as a Cd source, although they have the same hcp structure. The roses are composed of a number of nano-flakes in clusters. But for the spikes and cauliflowers, they compose of round nano-particles as fundamental. The spikes grew by the rapid assemblage of nano-particles in some specified directions, the cauliflowers by the assemblage of nano-particles in all directions at almost the same rates. These show that S sources dominated CdCl₂.2H₂O. Different product morphologies were influenced by S sources which have different structure formulas. Nucleation and growth of the particles can play roles in the morphologies. The crystal growth of some preferred structure or planes relates to the surface energy of the planes in the specified condition. The planes with

lower surface energy dominate those with higher surface energy. It is described as the shape selective surface absorption process [12]. The amount of starting agents in the solution also has the influence on different orientation of the particles which reflects nucleation and growth of the crystals. The orientation was increased by increasing in the amount of starting agents [13]. Apart from the above, crystal growth is influenced by the solubility of the precursors in the particular solvent and synthesized temperature which have the influence on the morphologies [12]. Polarities and boiling points of solvents [14], pH values of the solutions and others can play a role in the shapes and sizes due to the different rates of nucleation and growth. The products with different morphologies were also produced when different Cd sources reacted with CH₃CSNH₂. TEM images (Fig 5) show that the products compose of a number of nano-particles which clustered together at random. At present, nano-flakes and nano-particles are the fundamental particles of the products. The nano-flakes were formed by stacking hcp unit cells aside. There were some hcp unit cells stacked up as well, but its rate was the slowest. The nanoparticles were formed by the assemblage of unit cells (hcp for the spikes and cauliflowers, cubic for nano-particles in clusters). Growth of the nano-particles in all directions are at the same rates. The fundamental particles may contain some defects, due to the microwave vibration frequency, internal stress and others.

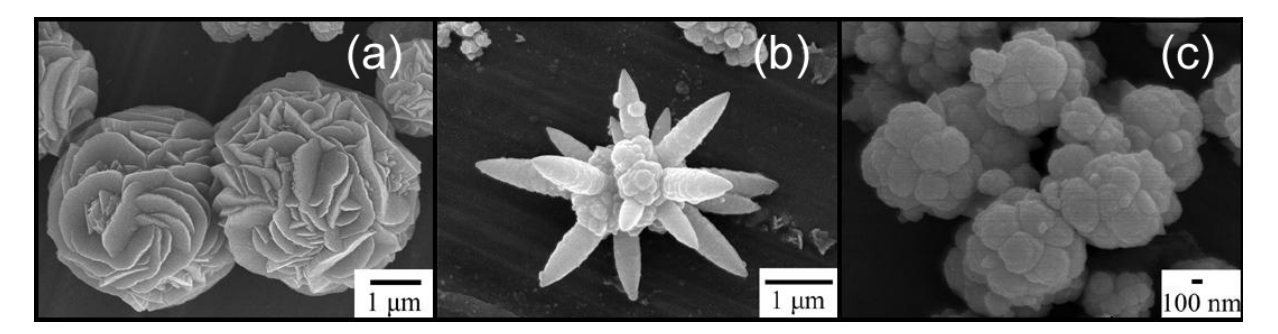


Fig 4. SEM images of the products prepared using (a) CdCl₂.2H₂O + CH₃CSNH₂, (b) CdCl₂.2H₂O + CH₅N₃S, and (c) CdCl₂.2H₂O + CH₆N₄S at 600 W for 9 cycles.

SAED patterns (Fig 5) show bright concentric rings corresponding to diffraction planes of the crystalline products. The rings are diffuse and hollow showing that the products composed of very fine particles. The values of interplanar spaces were calculated [15] using diameters of the diffraction rings measured from the patterns on the films, and compared with those of the JCPDS software [7]. The diffraction patterns correspond to CdS (cubic). HRTEM images (Fig 6) show the (111) plane of CdS (cubic) which are aligned in systematic array. There are several domains in the images. Each of them, belonging to a cluster of nano-particles, composes of a number of planes aligning in the same direction. By using XRD spectra in Fig 2b and Bragg's law for diffraction, calculated interplanar spaces of (111) plane [0.3476 nm for Cd(CH₃COO)₂.2H₂O + CH₃CSNH₂, and 0.3469 nm for Cd(NO₃)₂.4H₂O + CH₃CSNH₂] are very close to the corresponding values (0.3521 and 0.3424 nm) measured from Fig 6.

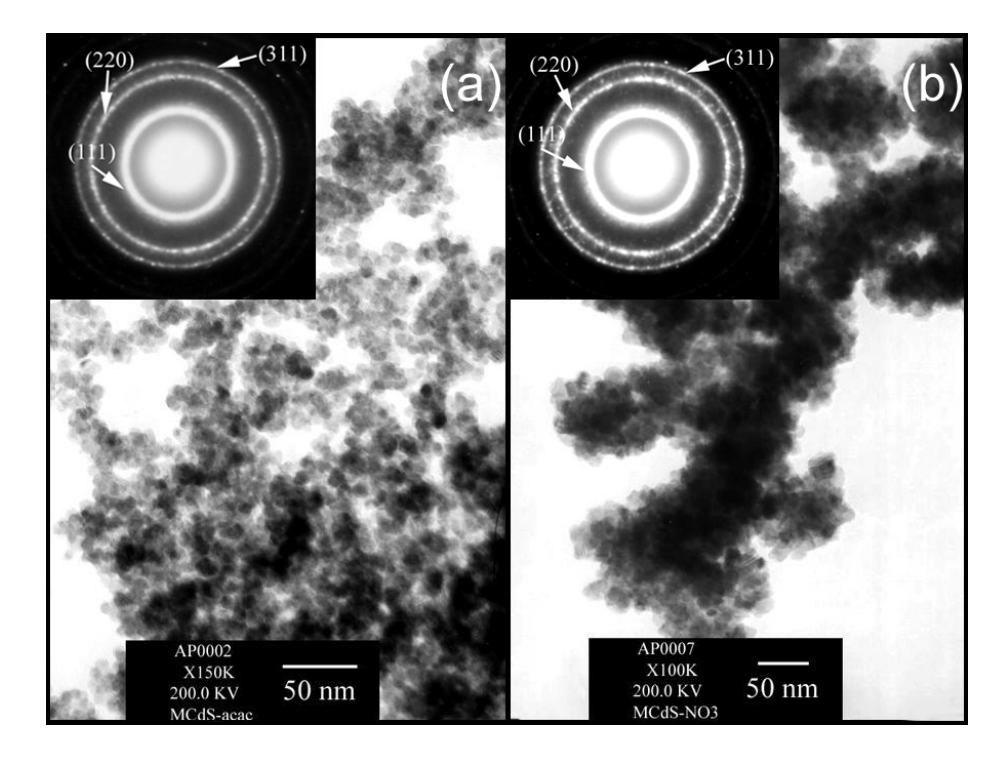


Fig 5. TEM images and SAED patterns of the products prepared using (a) $Cd(CH_3COO)_2.2H_2O + CH_3CSNH_2$ and (b) $Cd(NO_3)_2.4H_2O + CH_3CSNH_2$ at 600 W for 9 cycles.

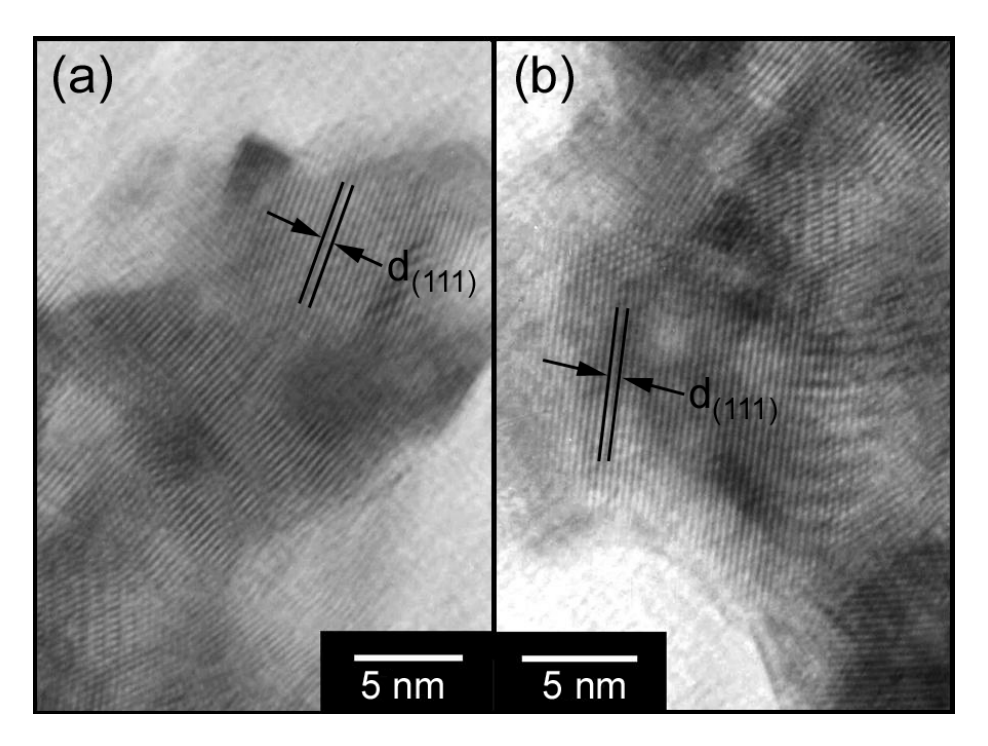


Fig 6. Interplanar space (d_{111}) of the products prepared using (a) $Cd(CH_3COO)_2.2H_2O + CH_3CSNH_2$, and (b) $Cd(NO_3)_2.4H_2O + CH_3CSNH_2$ at 600 W for 9 cycles.

For the present research, Cd and S sources have the influence on the nucleation and growth of the crystals. Phase with the lowest Gibbs free energy is thermodynamically stable, and has more chance to exist in the process [16]. These reflect the product morphologies. Apart from the above, crystal growth is influenced by the solubility of the precursors in the particular solvent and synthesized conditions which reflect the morphologies [12]. Higher microwave powers and exposure times also play the role in the product morphologies by enlarging the size of the roses that synthesized using CdCl₂.2H₂O and CH₃CSNH₂. Microwave radiation is able to reduce time scales of the reactions, and can rapidly lead to very high temperatures which have the influence to accelerate the reaction process.

References

- 1. A.V. Murugan, R.S. Sonawane, B.B. Kale, S.K. Apte, A.V. Kulkarni, Microwave-solvothermal synthesis of nanocrystalline cadmium sulfide, Mater. Chem. Phys. 71(2001)98-102
- 2. W. Qingqing, X. Gang, H. Gaorong, Solvothermal synthesis and characterization of uniform CdS nanowires in high yield, J. Solid State Chem. 178(2005)2680-2685
- 3. Q. Zhao, L. Hou, R. Huang, S. Li, Surfactant-assisted growth and characterization of CdS nanorods, Inorg. Chem. Comm. 6(2003)1459-1462
- 4. H. Yang, C. huang, X. Li, R. Shi, K. Zhang, Luminescent and photocatalytic properties of cadmium sulfide nanoparticles synthesized via microwave irradiation, Mater. Chem. Phys. 90(2005)155-158

- 5. L. Wang, L. Chen, T. Luo, Y. Qian, A hydrothermal method to prepare the spherical ZnS and flower-like CdS microcrystallites, Mater. Lett. 60(2006)3627-3630
- 6. T. Thongtem, A. Phuruangrat, S. Thongtem, Free surfactant synthesis of microcrystalline CdS by solvothermal reaction, Mater. Lett., 61(2007)3235-3238
- 7. Powder Diffract. File, JCPDS Internat. Centre Diffract. Data, PA 19073-3273,U.S.A. (2001)
- 8. V. Sivasubramanian, A.K. Arora, M. Premila, C.S. Sundar, V.S. Sastry, Optical properties of CdS nanoparticles upon annealing, Physica E 31(2006)93-98
- 9. J. Lee, Raman scattering and photoluminescence analysis of B-doped CdS thinfilms, Thin Solid Films 451-452(2004)170-174
- 10. C. Li, X. Yang, B. Yang, Y. Yan, Y. Qian, Growth of microtubular complexes as precursors to synthesize nanocrystalline ZnS and CdS, J. Cryst. Growth, 291(2006)45-51
- 11. O. Zelaya-Angel, F. de L. Castillo-Alvarado, J. Avendaño-López, A. Escamilla-Esquivel, G. Contreras-Puente, R. Lozada-Morales, G. Torres-Delgado, Raman studies in CdS thin films in the evolution from cubic to hexagonal phase, Solid State Comm. 104(1997)161-166
- 12. S. Biswas, S. Kar, S. Chaudhuri, Growth of different morphological features of micro and nanocrystalline manganese sulfide via sovothermal process, J. Cryst. Growth 299(2007)94-102
- 13. Y.C. Zhang, X.Y. Hu, T. Qiao, Shape-controlled synthesis of CuS nanocrystallites via a facile hydrothermal route, Solid State Comm. 132(2004)779-782
- 14. J. Lu, Q. Han, X. Yang, L. Lu, X. Wang, Microwave-assisted synthesis and characterization of 3D flower-like Bi₂S₃ superstructures, Mater. Lett. 61(2007)2883-2886

- 15. T. Thongtem, S. Kaowphong, S. Thongtem, Malic acid complex method for preparation of LiNiVO₄ nano-crystallites, J. Mater. Sci. 42(2007)3923-3927
- 16. K. Sopunna, T. Thongtem, M. McNallan, S. Thongtem, Formation of titanium nitride on γ -TiAl alloys by direct metal-gas reaction, J. Mater. Sci., 41(2006)4654-4662

Formation of CuS with flower-like, hollow spherical, and tubular structures

using the solvothermal-microwave process

Abstract

CuCl₂·2H₂O and CH₃CSNH₂ were dissolved in ethylene glycol, and followed by the

addition of NaOH to form solutions with different pH values. Reactions proceeded in

surfactant-free solutions contained in an acid digestion bomb using a microwave

irradiation at different conditions. Pure CuS (hcp) with flower-like, hollow spherical,

and tubular structures were detected, and had the same vibration wavenumber at

474 cm⁻¹. They displayed two emission peaks at 411, and 432 nm. Formation of CuS

with different morphologies was proposed according to the analytical results.

Keywords: Surfactant-free solutions; Solvothermal-microwave process; CuS;

Flower-like structure; Hollow spheres; Tubular structure

Introduction

CuS with flower-like, hollow spherical, and tubular structures in nanometer and

micrometer sizes is a very attractive material due to its specific structures and novel

properties. It has a wide variety of applications, such as solar cells, superionic

materials, and optical filters [1]. CuS was produced by different methods, such as

spray pyrolysis [2], solvothermal process [3], sonochemistry [4], and microwave

synthesis [5]. Surfactants, templates, and other additives were used to control the

morphologies in most processes. For solution in a digestion bomb, microwave

heating is very attractive method due to focusing a large amount of energy into the chemicals under high pressure. The purpose of the research is to produce CuS with flower-like, hollow spherical, and tubular structures in surfactant-free solutions with different pH values using the solvothermal-microwave process in an acid digestion bomb.

Experiment

The 5 mmol each of $CuCl_2 \cdot 2H_2O$ and CH_3CSNH_2 was dissolved in 40 mL ethylene glycol. A pH was adjusted using NaOH. The solutions were stirred at ambient temperature. The reactions proceeded in an acid digestion bomb using 180 W cyclic microwave irradiation for 24 and 72 cycles (1,200 and 3,600 s). Each cycle was 50 s long. It was on for x s and off for 50 - x s. The irradiation percents for every cycle were 2x = 20, 30, 50, and 60 %. An increase in the irradiation percent of each cycle had an influence on the system by raising its temperature. The number of cycles is the time that the reaction proceeded in both the on and off states. At the conclusion of the test, the products were washed with water and ethanol, dried at 80 °C for 12 h, and intensively analyzed.

Results and discussion

To determine the phase of the products, their XRD spectra (Fig. 1) were compared with that of the JCPDS software (reference code: 78-0876) [6], and specified as CuS (hcp). No other characteristic peaks of impurities were detected although they were produced using different conditions. The degrees of crystallinity were increased with the increase in the irradiation percents of each cycle, and numbers of heating cycles (Fig. 1a), identified by the narrower and higher peaks. When more energy was

supplied to the system, atoms violently vibrated and aligned in periodic array in the lattice. Different pH values (Fig. 1b) did not play a significant role in the diffraction peaks, and degree of crystallinity.

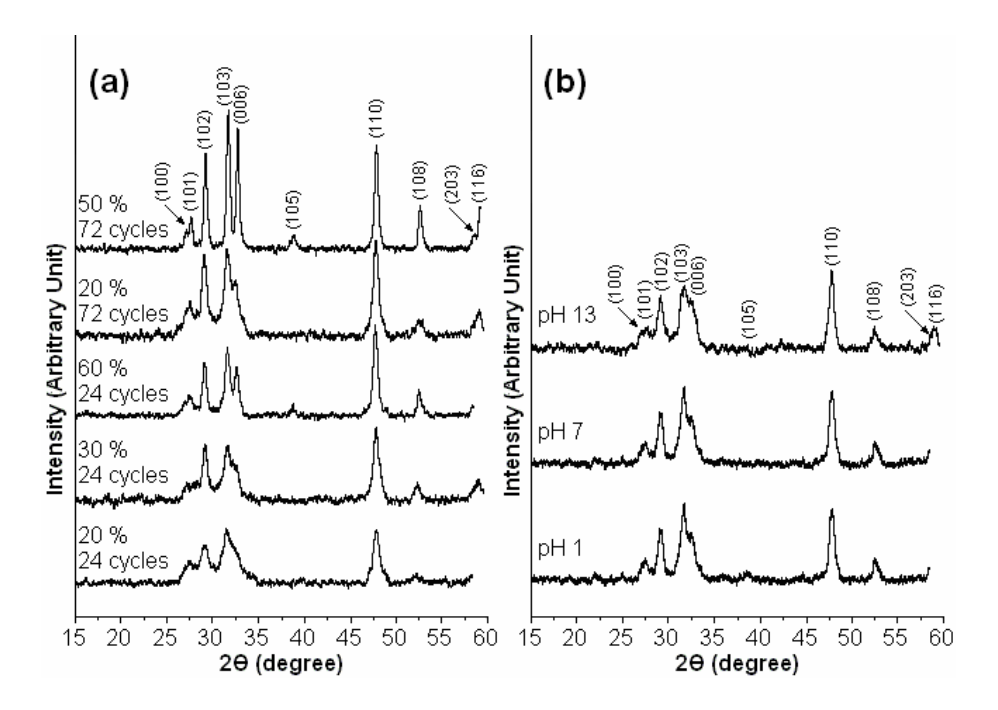


Fig. 1. XRD spectra of the products produced using (a) an extremely low pH value at different irradiation percents of each cycle and numbers of heating cycles, and (b) different pH values at 50 % irradiation for 24 cycles.

To produce CuS in an acid digestion bomb, CuCl₂·2H₂O and CH₃CSNH₂ were mixed in ethylene glycol and stirred at ambient temperature. The existence of precipitates (copper-thioacetamide complex) which were subsequently decomposed by the microwave irradiation [7].

$$CuCl_2 + 2CH_3CSNH_2$$
 \longrightarrow $[Cu(CH_3CSNH_2)_2]^{2+} + 2Cl^{-}$

Microwave irradiation

To show that copper-thioacetamide complex was definitely produced. FTIR spectra (Fig. 2) of CH₃CSNH₂ and the precipitates (copper-thioacetamide complex, [Cu(CH₃CSNH₂)₂]Cl₂) were analyzed. For CH₃CSNH₂, C=S stretching vibrations were detected at 735 and 984 cm⁻¹, and N-H stretching vibrations at 3,178 and 3,443 cm⁻¹. Corresponding vibrations of the complex were at 710 and 978 cm⁻¹ for C=S stretching, and 3,153 and 3,305 cm⁻¹ for N-H stretching. The two C=S peaks of CH₃CSNH₂ became weakened. The 735 cm⁻¹ C=S vibration tended to split into two peaks. Both C=S and N-H peaks shifted to the lower wavenumbers due to the reduction in the vibration constants and bonding energies of C=S and N-H. These were caused by the reduction in the electronegativities of N and S atoms which were the result of partial donation of lone pair electrons of N and S atoms to the vacant d orbital of Cu²⁺ ions [8]. C-N peaks of CH₃CSNH₂ and the complex were detected at the same wavenumbers [8] of 1,411 and 1,496 cm⁻¹. The peaks remained stationary but became weakened and broadened, when they were in the complex. Changes in the nature of C=S, C-N, and N-H bonds are the evidence of the complex formation [8,9]. In addition, the complex was analyzed using CHON/S analyzer and AAS. It is composed of 27.01 wt% Cu, 14.28 wt% C, 3.04 wt% H, 22.29 wt% S, and 8.21 wt%

N. For 100 wt% complex, mole ratios of Cu : C : H : S : N : Cl are 1.42 : 3.96 : 10.05 : 2.32 : 1.95 : 2.37, which are in accord with its formula.

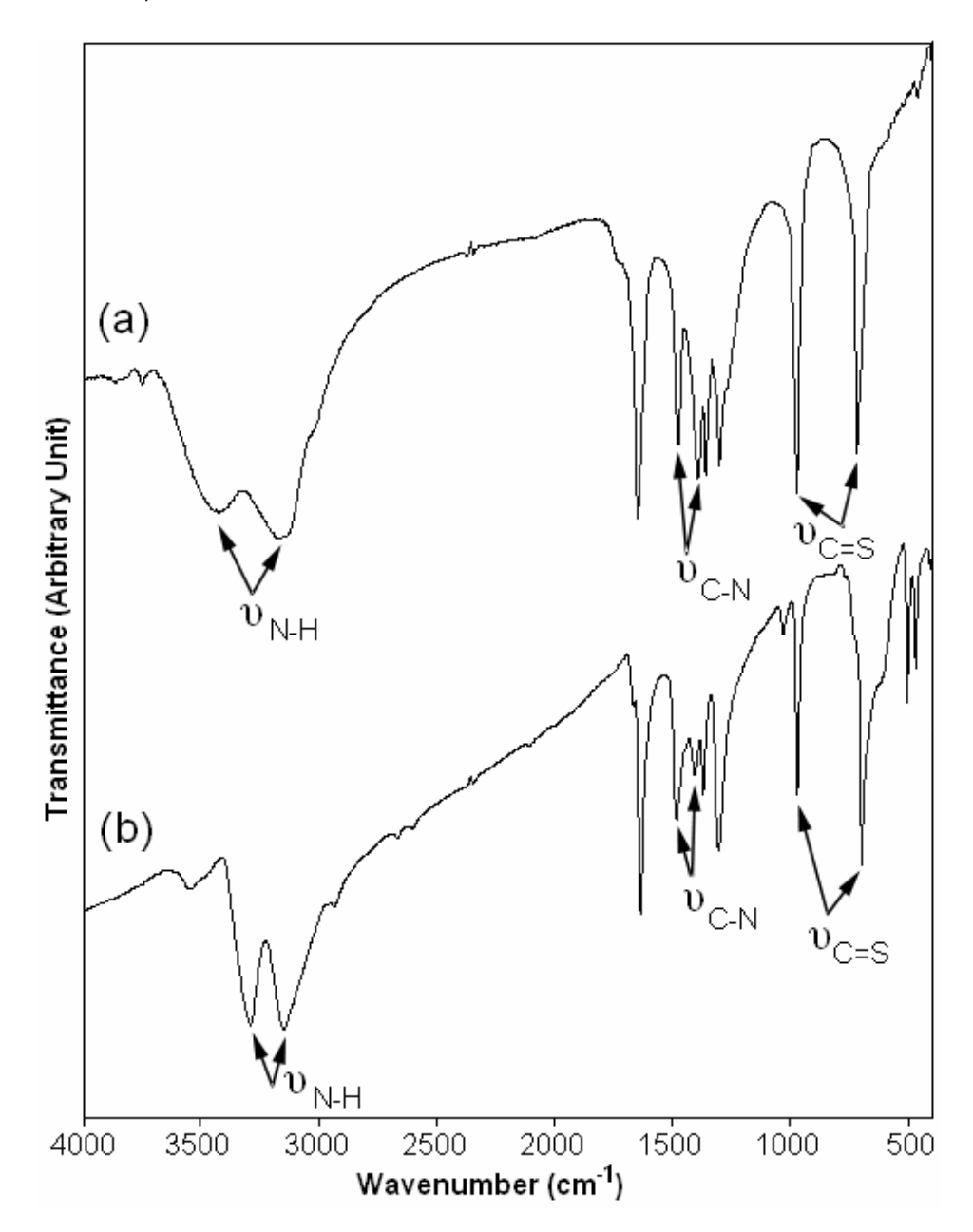


Fig. 2. FTIR spectra of (a) CH₃CSNH₂ and (b) [Cu(CH₃CSNH₂)₂]Cl₂.

Alternatively, CH_3CSNH_2 reacted with H_2O (crystal water in $CuCl_2 \cdot 2H_2O$ and trace water in ethylene glycol) to form H_2S [10]. Subsequently, H_2S combined with $CuCl_2$ to produce CuS. The reactions proceeded by the assistance of the microwave irradiation.

Microwave irradiation

$$CH_3CSNH_2 + H_2O$$
 $H_2S + CH_3(NH_2)C=O$

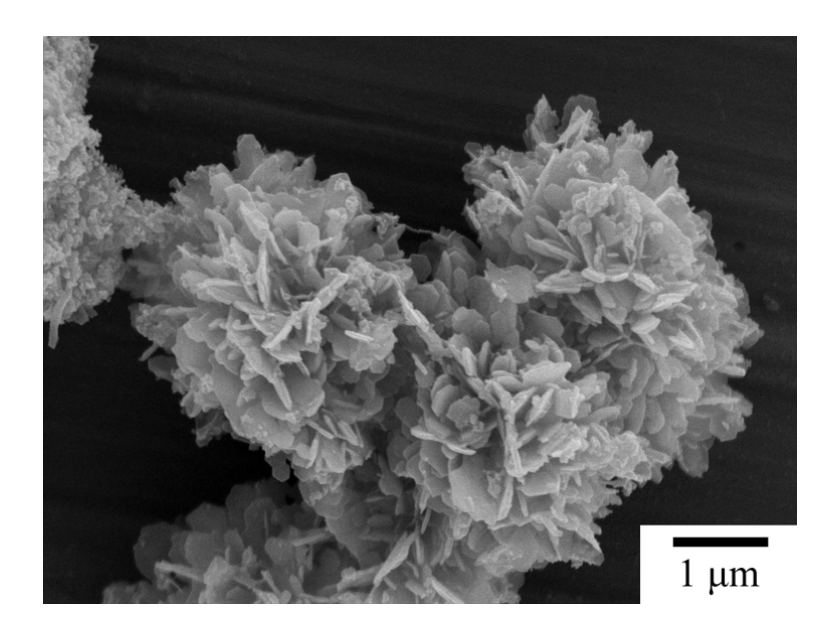
Microwave irradiation

 $H_2S + CuCl_2$
 $CuS (black) + 2HCl$

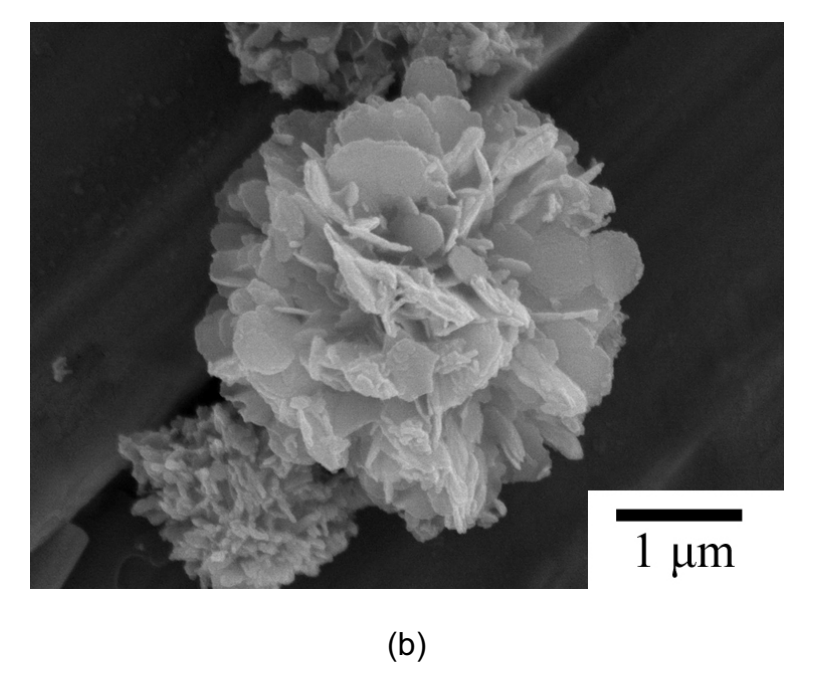
After the starting agents were mixed and stirred, the solution has the characteristic of strong acid that the pH was extremely low (very close to zero). Once CuS nuclei formed in the digestion bomb by the assistance of the microwave irradiation. They were not fully developed (nascent) and grew very rapidly via the diffusion process. When NaOH was slowly added into the solutions, different pH values can play a role in the nucleation and growth processes.

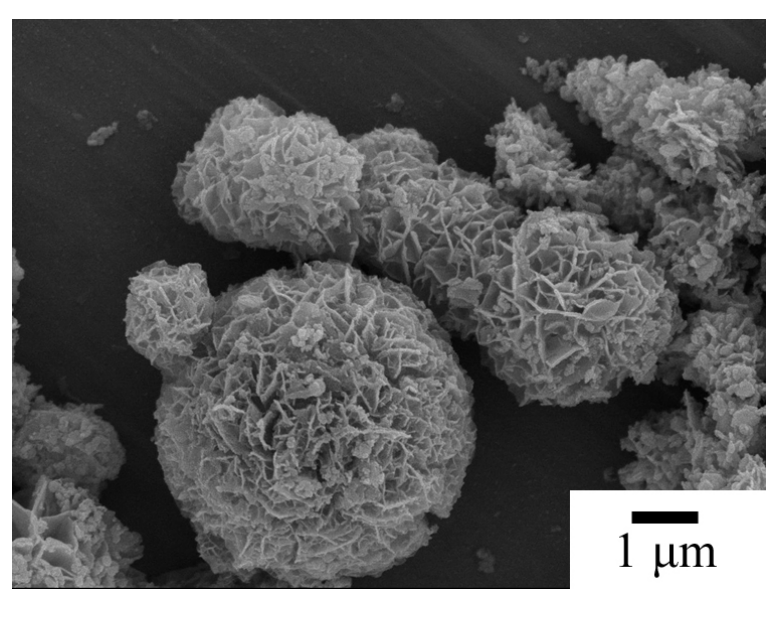
At extremely low pH value, the morphologies (Fig. 3) were influenced by the irradiation percents and cycles. At 20 % irradiation and 24 cycles (Fig. 3a), the product composed of a number of nano-plates in clusters shaped like flowers, and became larger when the irradiation time was prolonged to 72 cycles (Fig. 3b). Their particle-sized distributions will be discussed in more detail later in this section. To form plate-like particles, the stacking rate of hcp structure in the normal direction to the plates was the slowest. Plate-like formation and clustering simultaneously proceeded to produce flower-like products. At 30 and 60 % irradiation for 24 cycles (Figs. 3c and 3d), and 50 % irradiation for 72 cycles (Fig. 3e), the flowers are very similar to spheres. They were produced in different sizes showing that their initiation was different. There are more pores on the spheres at higher irradiation percents and

cycles. Some spheres were broken. During processing, the irradiation percents of each cycle were long enough to heat up the products to be at higher temperatures. The spheres became bigger due to the growth process. Further gas was produced inside. There was some gas diffused out of the spheres as well. The evolution of the gas seems to be from the following. (1) Decomposition of ethylene glycol and acetamide (CH₃(NH₂)C=O). (2) Dehydration of ethylene glycol with acid served as a catalyst. Acetaldehyde developed [11], and further combined with oxygen to form CO₂ and water. When the pressure inside the spheres was high enough, fracture ultimately occurred and holes appeared. Some spheres were broken but some were not, depending on the number of defects in their shells, initiation time, pressure inside the spheres and others. Both the irradiation percents and cycles can play the important roles in the gas formation leading to the explosion process.



(a)





(c)

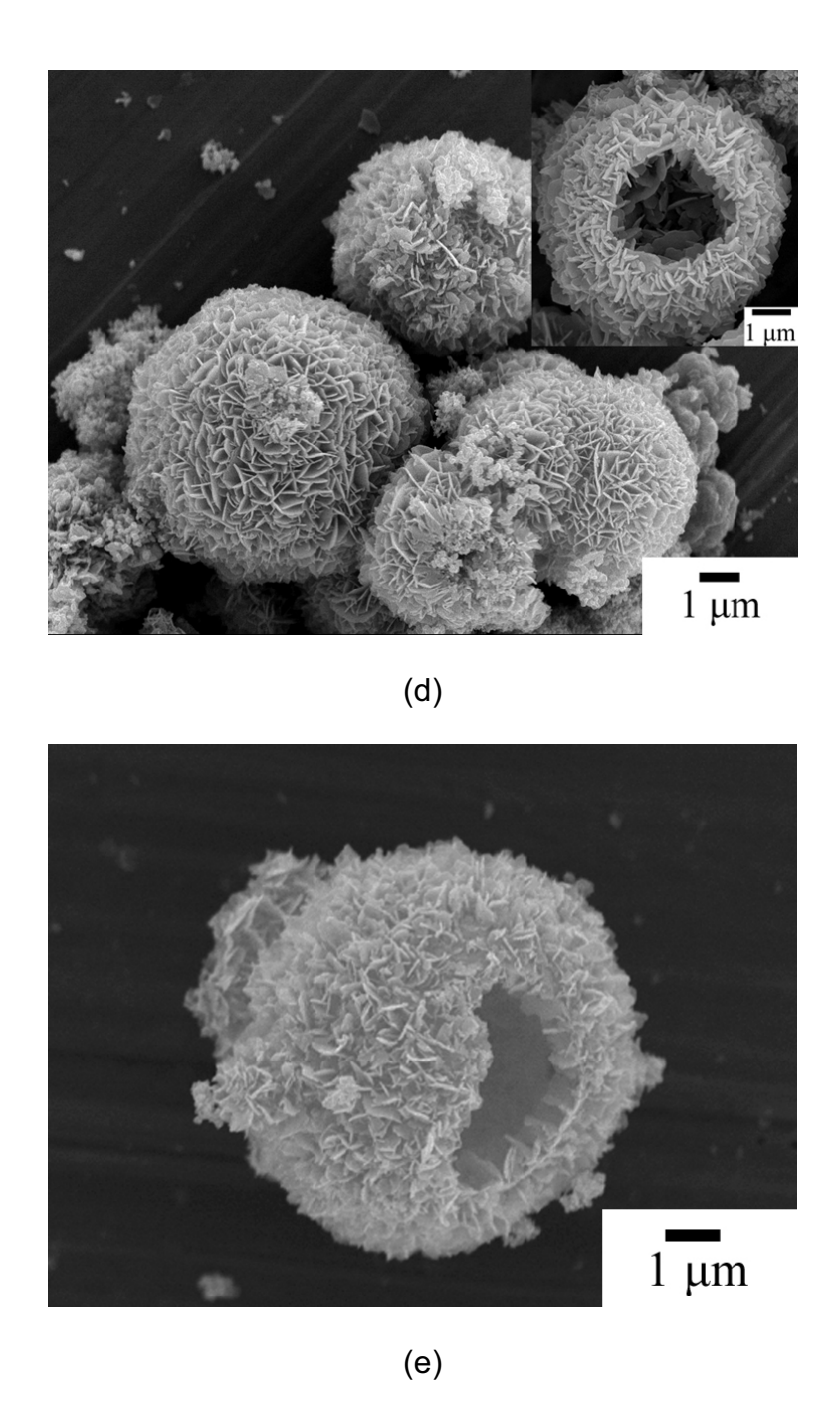
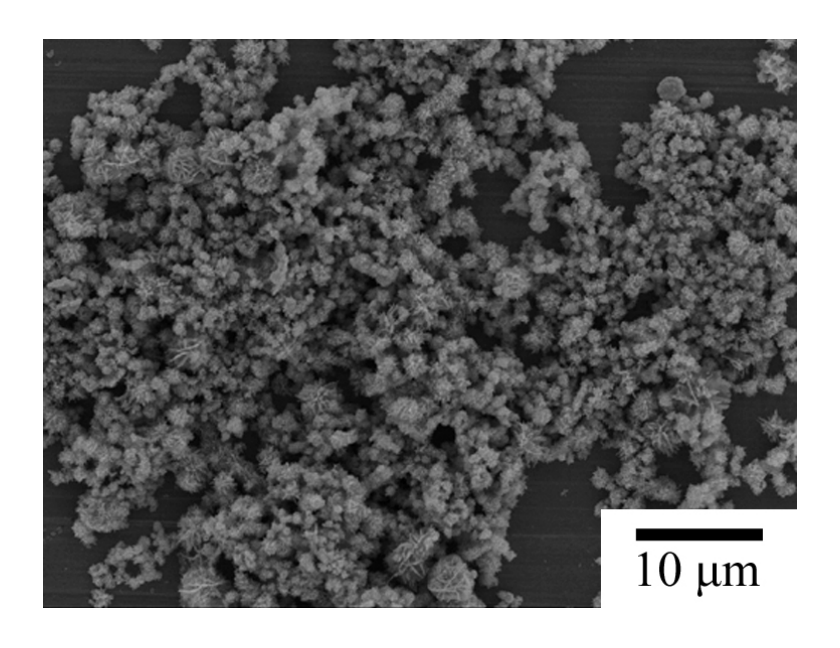


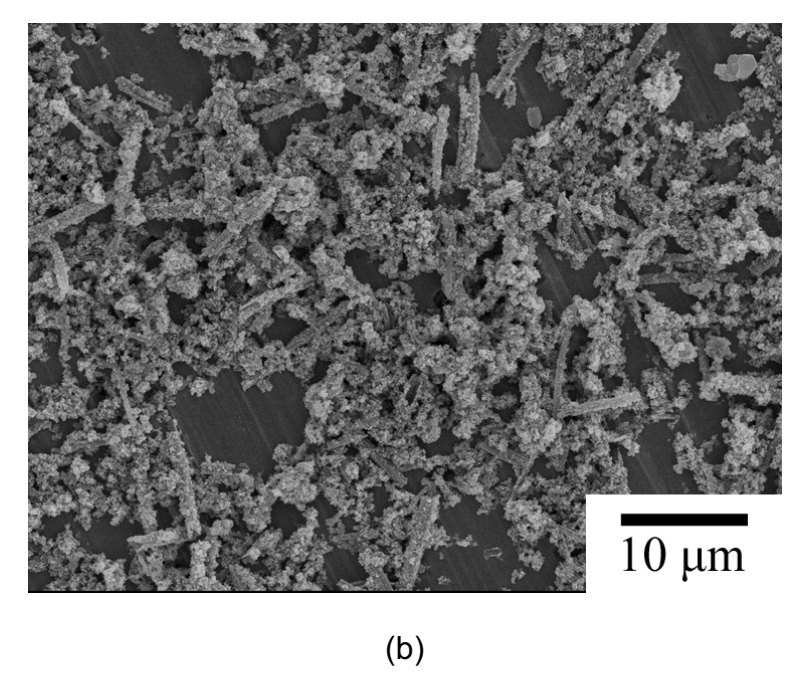
Fig. 3. SEM images of the products produced using an extremely low pH value at (a) 20 % irradiation for 24 cycles, (b) 20 % irradiation for 72 cycles, (c) 30 % irradiation for 24 cycles, (d) 60 % irradiation for 24 cycles, and (e) 50 % irradiation for 72 cycles.

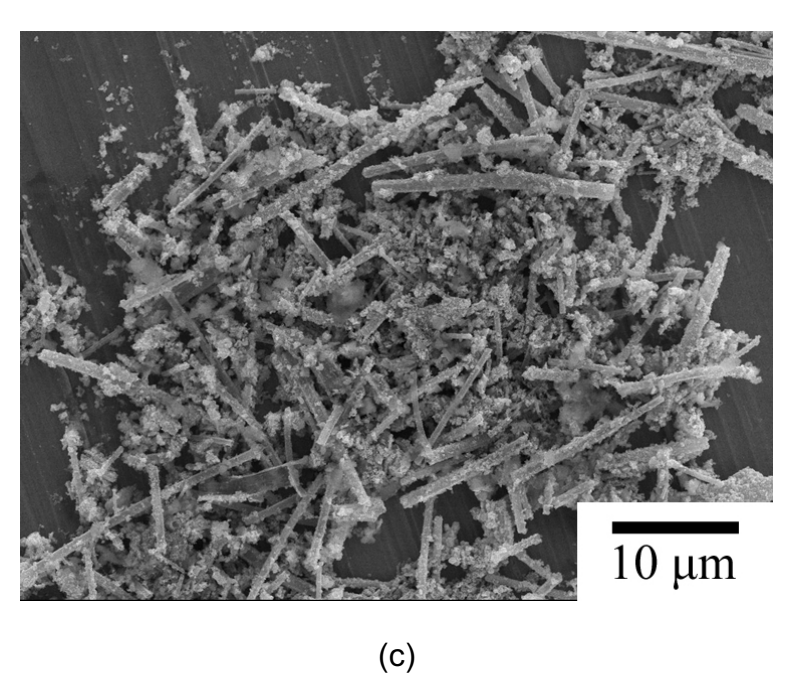
When NaOH was slowly added into the solutions (Fig. 4), the pH values slowly increased. At a pH of 1, 50 % irradiation, and 24 cycles (Fig. 4a), the products were clusters of nano-sized particles. OH ions seem to have the influence on their

nucleation and growth. No flower-like product existed, but some plates were left in the solution. At higher pH values (Figs. 4b and 4c), more nano-sized and less plate-like particles existed. Simultaneously, the nano-sized particles began to assemble into a hollow object in the shape of a tube. The degree of roughness on the side walls is higher than that at the ends. At the present stage, there are a number of sites for OH⁻ ions to adsorb on outside walls. It implies that concentration of OH⁻ ions adsorbing on outside walls is the highest. OH⁻ layer shields the tubular wall from the deposition of nano-sized particles. Therefore, clustering in the radial direction of the tubes is limited to some range. Growth proceeded only in the axial direction. A number of the tubes were produced. They were increased with the increase in the pH values. At a pH of 13 (Fig. 4d), a great number of the tubes were detected. Its enlarged SEM image (Fig. 4e) shows the nano-size particles assembled as tubular structure.



(a)





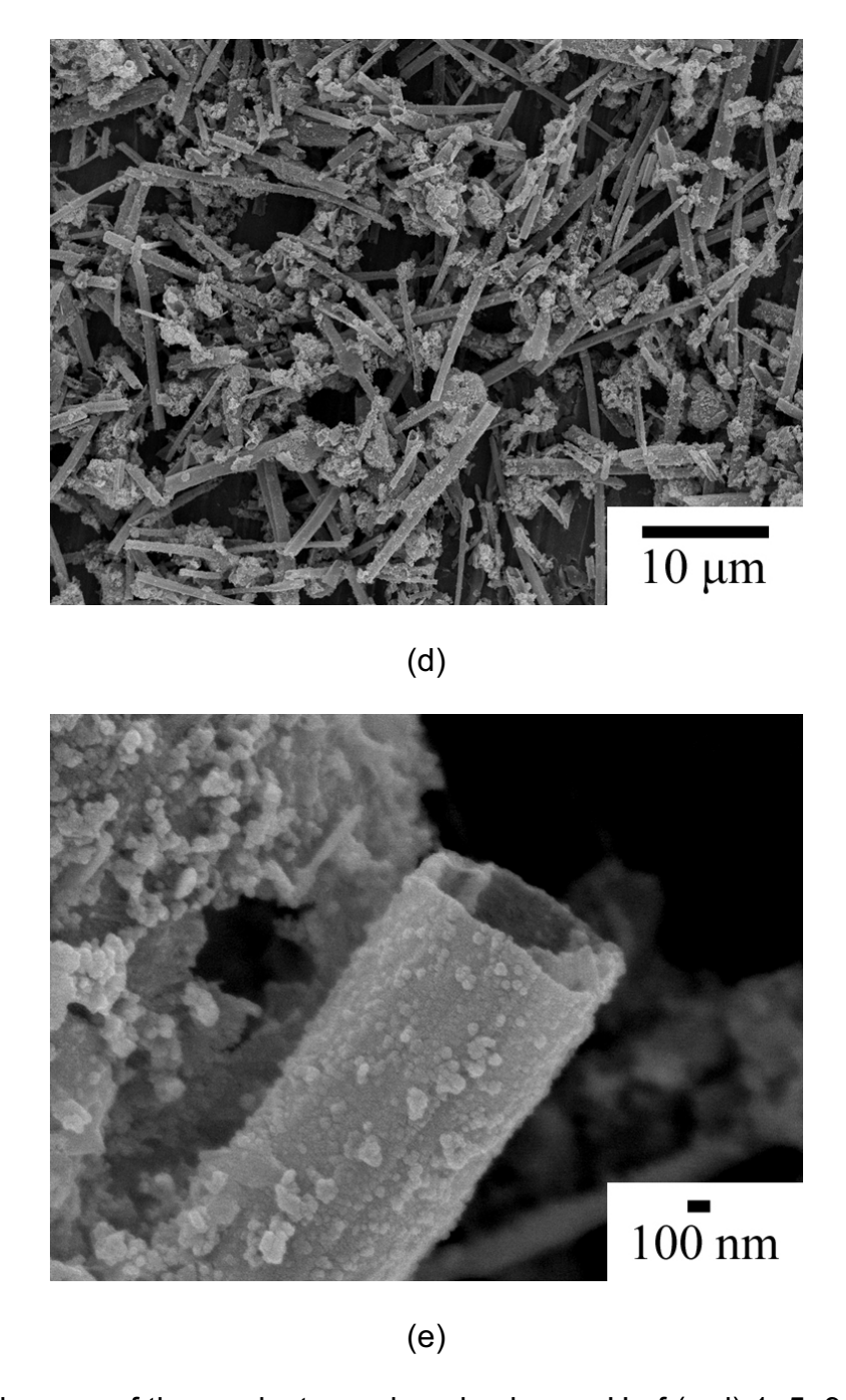


Fig. 4. SEM images of the products produced using a pH of (a-d) 1, 5, 9 and 13 at 50 % irradiation for 24 cycles, respectively. [(e) is the enlarged image of (d).]

TEM image (Fig. 5) shows different sizes of tubular structure composing of nanosized particles. Some particles existed as clusters. The tubes are 82 - 574 nm in diameter, and are as long as 6,420 nm (result not shown). Some irregular shapes and sizes of defects were detected on the tubular surfaces. SAED pattern (Fig. 5) shows eight concentric rings. They are diffuse showing that the tubes composed of nano-sized particles. Interplanar spaces were calculated [12,13] and compared with those of the JCPDS software [6]. The rings correspond to (100), (103), (006), (105), (110), (108), (203), and (116) planes, and reveal the presence of CuS (hcp).

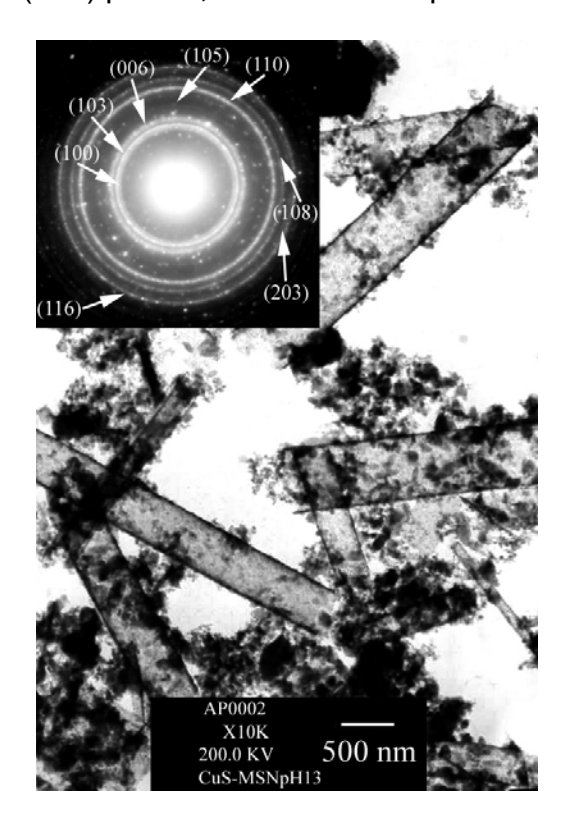


Fig. 5. TEM image and SAED pattern of the product produced using a pH of 13 at 50 % irradiation for 24 cycles.

Particle-sized distributions of the flower-like products produced using an extremely low pH value at 20 % irradiation for 24 and 72 cycles are shown in Fig. 6. The sizes are 198 ± 32 nm and 775 ± 167 nm for 24 and 72 cycles, respectively. Size distributions of the flower-like particles are over the range 142 - 295 nm for 24 cycles, and 459 - 1,281 nm for 72 cycles. Numbers of the cycles can play a role in the range of size distributions. Cumulative frequency shows that the particles were counted and arranged from the smallest value. It increased in a smooth monotone, showing that particle-sized distribution shapes like a bell.

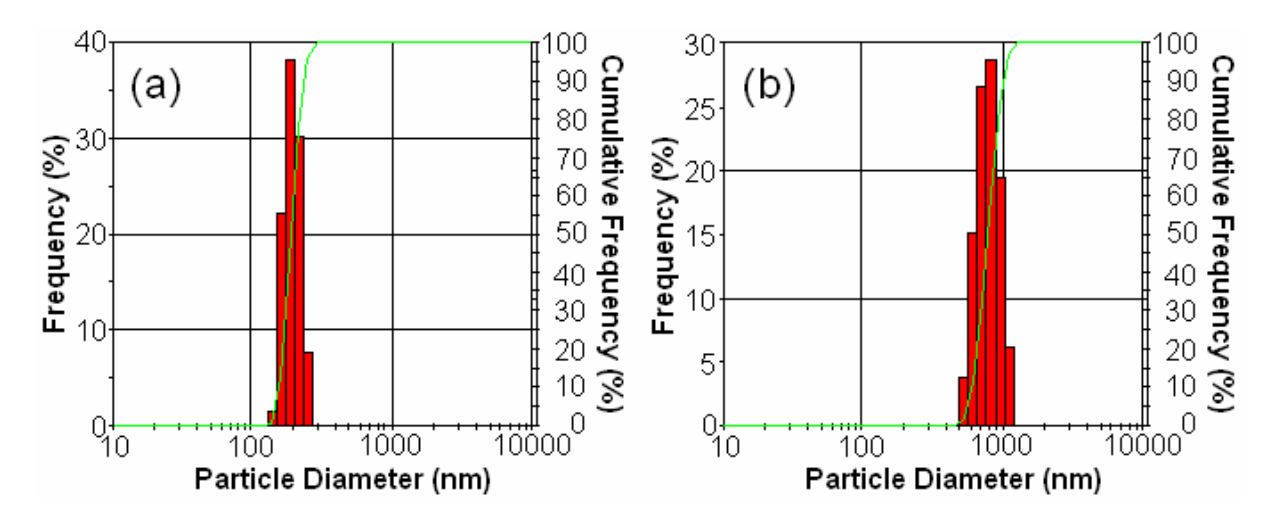


Fig. 6. Particle-sized distributions of the flower-like products produced using an extremely low pH value at 20 % irradiation for (a) 24 cycles, and (b) 72 cycles.

Raman spectra (Fig. 7) are very sharp, showing that lattice atoms are aligned in the periodic array. Their vibrations are in the same wavenumbers at 474 cm⁻¹, corresponding to lattice vibrations. The present results are in accord with those of CuS thin films [14].

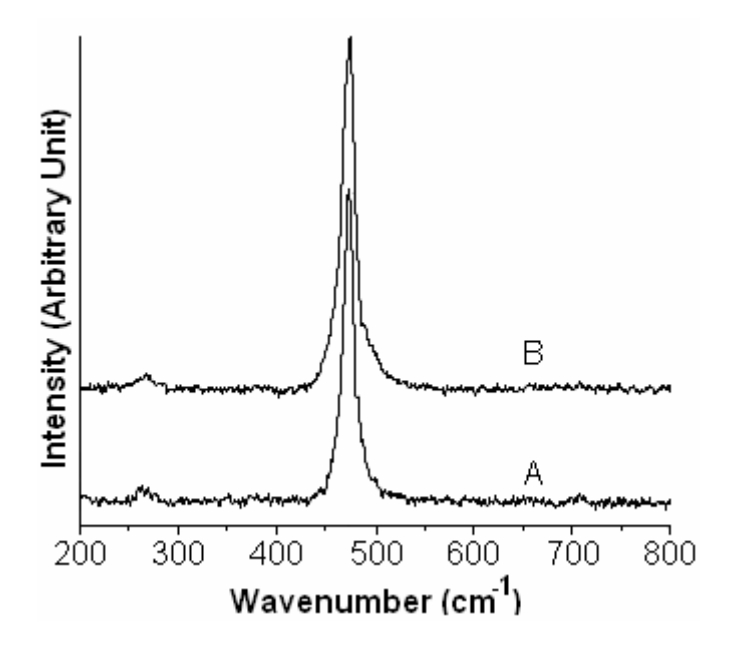


Fig. 7. Raman spectra of the products produced using (A) an extremely low pH value at 50 % irradiation for 72 cycles, and (B) a pH of 13 at 50 % irradiation for 24 cycles.

Photoluminescent (PL) emission of CuS dispersed in absolute ethanol (0.2 mg/mL) was determined at ambient temperature using an excitation wavelength of 202 nm, and is shown in Fig. 8. The spectra are broad and the two emission peaks are at 411 and 432 nm. The results are in accord with the emission peaks of CuS at 414 and 437.5 nm [3]. Their intensities are influenced by several parameters such as shapes, sizes, and crystallinities, which were controlled by synthesis conditions. For an extremely low pH value (A-D), PL intensities were increased with the increase in the irradiation percents of each cycle and numbers of heating cycles. The intensity was the highest at 50 % irradiation, and 72 cycles (D). For the pH of 1, 7 and 13, at 50 % irradiation for 24 cycles (E-G), PL intensities were increased with the increase in the pH values, until to the highest at the pH of 13 (G). For present analysis, the tubular product (at the pH of 13, 50 % irradiation, and 24 cycles) displayed the most efficient PL.

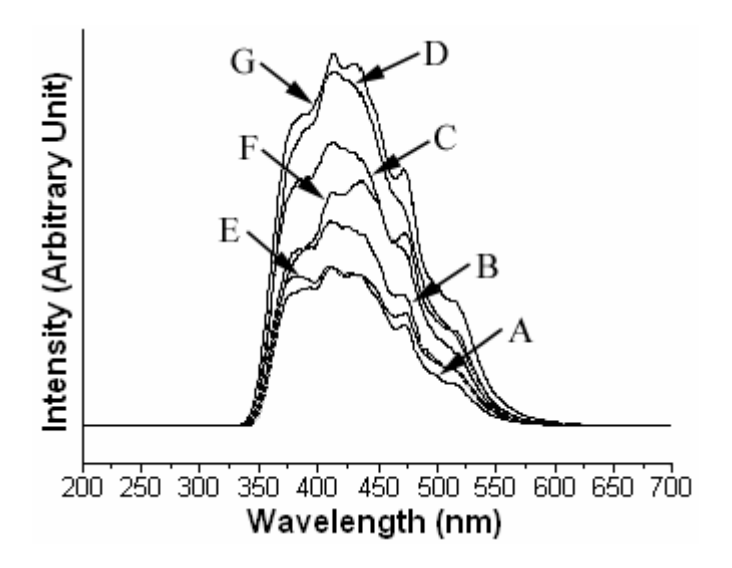


Fig. 8. PL emission of the products produced using (A-D) an extremely low pH value at 20 % irradiation for 24 cycles, 60 % irradiation for 24 cycles, 20 % irradiation for 72 cycles, and 50 % irradiation for 72 cycles, and (E-G) the pH of 1, 7 and 13 at 50 % irradiation for 24 cycles, respectively.

Conclusions

CuS with flower-like, hollow spherical, and tubular structures was successfully produced by solvothermal-microwave process at different conditions in an acid digestion bomb. CuS (hcp) was detected using XRD and SAED. Its Raman wavenumber is at 474 cm⁻¹. Different morphologies were characterized using SEM and TEM, ranging from flower-like in a solution with extremely low pH to tubular in a pH of 13. PL emission peaks are at 411 and 432 nm. Their intensities are influenced by several parameters such as shapes, sizes, and crystallinities, controlled by synthesis conditions. The product with tubular structure exhibits best PL efficiency. Formation of CuS with different morphologies was also proposed.

References

- [1] Y. Ni, R. Liu, X. Cao, X. Wei, J. Hong, Mater. Lett., 61 (2007) 1986-1989
- [2] J. Madarász, M. Okuya, S. Kaneko, J. Europ. Ceram. Soc., 21 (2001) 2113-2116
- [3] S. Ou, Q. Xie, D. Ma, J. Liang, X. Hu, W. Yu, Y. Qian, Mater. Chem. Phys., 94 (2005) 460-466
- [4] J.Z. Xu, S. Xu, J. Geng, G.X. Li, J.J. Zhu, Ultrason. Sonochem., 13 (2006) 451-454
- [5] X.H. Liao, J.J. Zhu, H.Y. Chen, Mater. Sci. Engin. B, 85 (2001) 85-89
- [6] Powder Diffract. File, JCPDS Internat. Centre Diffract. Data, PA 19073-3273, U.S.A., (2001)

- [7] D. Chen, K. Tang, G. Shen, J. Sheng, Z. Fang, X. Liu, H. Zheng, Y. Qian, Mater. Chem. Phys., 82 (2003) 206-209
- [8] J.Y. Gong, S.H. Yu, H.S. Qian, L.B. Luo, X.M. Liu, Chem. Mater., 18 (2006) 2012-2015
- [9] T. Thongtem, A. Phuruangrat, S. Thongtem, J. Mater. Sci., 42 (2007) 9316-9323
- [10] J. Zhu, M. Zhou, J. Xu, X. Liao, Mater. Lett., 47 (2001) 25-29
- [11] W.B. Smith, Tetrahedron, 58 (2002) 2091-2094
- [12] T. Thongtem, A. Phuruangrat, S. Thongtem, Mater. Lett., 60 (2006) 3776-3781
- [13] T. Thongtem, S. Kaowphong, S. Thongtem, J. Mater. Sci., 42 (2007) 3923-3927
- [14] S.Y. Wang, W. Wang, Z.H. Lu, Mater. Sci. Engin. B, 103 (2003) 184-188

Influence of cetyltrimethylammonium bromide on the morphology of AWO_4 (A = Ca, Sr) prepared by cyclic microwave irradiation

Abstract

AWO₄ (A = Ca, Sr) was prepared from metal salts [Ca(NO₃)₂.4H₂O or Sr(NO₃)₂], Na₂WO₄.2H₂O and different moles of cetyltrimethylammonium bromide (CTAB) in water by cyclic microwave irradiation. The structure of AWO₄ was characterized by X-ray diffraction (XRD) and selected area electron diffraction (SAED). Transmission electron microscopy (TEM) and scanning electron microscopy (SEM) revealed the presence of nanoparticles in clusters with different morphologies; spheres, peaches with notches, dumb-bells and bundles, influenced by CTAB. Six Raman vibrational peaks of scheelite structure were detected at 908, 835, 793, 399, 332 and 210 cm⁻¹ for CaWO₄ and 917, 833, 795, 372, 336 and 192 cm⁻¹ for SrWO₄, which are assigned as $v_1(A_g)$, $v_3(B_g)$, $v_3(E_g)$, $v_4(B_g)$, $v_2(A_g)$ and $v_{f.r.}(A_g)$, respectively. Fourier transform infrared (FTIR) spectra provided the evidence of W-O stretching vibration in [WO₄]²⁻¹ tetrahedrons at 793 cm⁻¹ for CaWO₄ and 807 cm⁻¹ for SrWO₄. The peaks of photoluminescence (PL) spectra were at 428-434 nm for CaWO₄, and 447-451 nm for SrWO₄.

Keywords: Cyclic microwave irradiation; Nanostructured AWO₄ (A = Ca, Sr); Spheres; Peaches with notches; Dumb-bells; Bundles

Introduction

Metal tungstates are classified into two groups with different crystal structures; scheelites (CaWO₄, SrWO₄, BaWO₄ and PbWO₄) and wolframites (MgWO₄, ZnWO₄, CdWO₄, etc.) [1]. Among the crystals with scheelite structures, CaWO₄ and SrWO₄ have attracted particular interest in a variety of studies such as stimulated Raman scattering technique [2], electrooptical property [3] and microwave application [4]. They were prepared by chemical bath deposition [5], Czochralski technique [6], solvothermal-mediated microemulsion method [7], metathetic reaction [8] and the evaporation of a polymer based metal-complex precursor solution [9]. In this study, the influence of CTAB on the morphologies of AWO₄ (A = Ca, Sr) prepared by cyclic

microwave irradiation was demonstrated. The reaction proceeded in an open system at atmospheric pressure without any further requirement of calcination. The process is very simple, attractive and novel by focusing large amount of microwave irradiation into the solutions to produce pure products.

Experiment

Different moles (M) of CTAB and 3 mM $Na_2WO_4.2H_2O$ were separately dissolved in 10 ml water and mixed. Subsequently, a solution of 3 mM $Ca(NO_3)_2.4H_2O$ or $Sr(NO_3)_2$ in 10 ml water was put in the mixture. The reactions cyclically proceeded using 300 W microwave for 10 min to produce AWO_4 (A = Ca, Sr). One cycle of the microwave irradiation consists of 10 s irradiation and 20 s interval. The products were washed with water and 95 % ethanol, and dried at 70 °C for 12 h.

Results and Discussion

XRD spectra of CaWO₄ and SrWO₄ prepared with different moles of CTAB are shown in Fig. 1. The spectra were compared with those of the JCPDS software (reference codes: 77-2234 and 85-0587) [10], and specified as AWO₄ (A = Ca, Sr). They have scheelite tetragonal structure and I4₁/a space-group symmetry [10]. Their strongest intensity peaks are at $2\theta = 28.88$ and 27.64 deg for CaWO₄ and SrWO₄, respectively, assigned to (112) plane. Calculated lattice parameters [11] for CaWO₄ (a = b = 0.5218 ± 0.0013 nm and c = 1.1316 ± 0.0022 nm) and SrWO₄ (a = b = 0.5417 ± 0.0007 nm and c = 1.1951 ± 0.0000 nm) are very close to those of the corresponding JCPDS software, and have the influence on their interplanar spaces. No other characteristic peaks of impurities were detected.

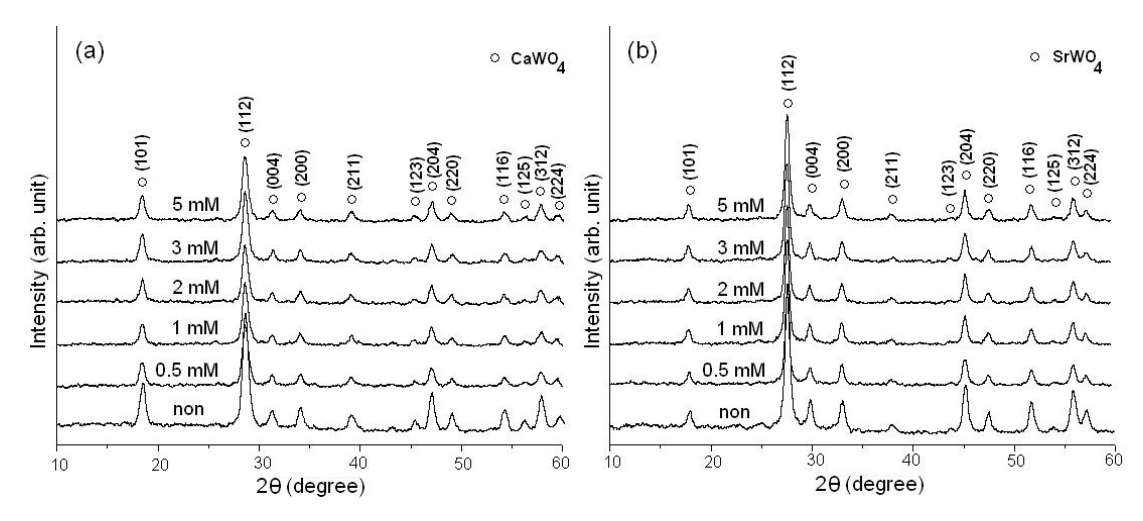


Fig. 1. XRD spectra of (a) CaWO₄ and (b) SrWO₄ prepared with different moles of CTAB.

Vibrations of AWO₄ are classified into two types, the internal and external modes [6]. The first belongs to the vibration inside [WO₄]²⁻ molecular units of which the centers of mass are stationary. The second is called lattice phonon which corresponds to the motion of A²⁺ cations and the rigid molecular units. In free space, [WO₄]²⁻ tetrahedrons have T_d symmetry [6,12]. Their vibrations compose of four internal modes (v₁(A₁), v₂(E), v₃(F₂) and v₄(F₂)), one free rotation mode (v_{f.r.}(F₁)), and one translation mode (F₂) [6]. In lattice space, the symmetry is reduced to S₄. All degenerative vibrations are split [6,12] due to the crystal field effect and Davydov splitting [6]. For tetragonal scheelite primitive cell (wavevector **k** = **0**) [6,13], there are 26 different vibrations ($\Gamma = 3A_g + 5A_u + 5B_g + 3B_u + 5E_g + 5E_u$) determined by group theory calculation [6,12]. Among them, $3A_g$, $5B_g$ and $5E_g$ vibrations are Ramanactive. Only $4A_u$ and $4E_u$ of the $5A_u$ and $5E_u$ vibrations are active in IR frequencies, and the others ($1A_u$ and $1E_u$) are acoustic vibrations. The $3B_u$ vibrations are silent modes [6,12].

For the present research, six different vibrations were detected on Raman spectra shown in Figs. 2a and 2b. Among them, $v_1(A_g)$, $v_3(B_g)$, $v_3(E_g)$, $v_4(B_g)$, $v_2(A_g)$ and $v_{f.r.}(A_g)$ are at 908, 835, 793, 399, 332 and 210 cm⁻¹ for CaWO₄, and 917, 833, 795, 372, 336 and 192 cm⁻¹ for SrWO₄, respectively. Each vibration mode is in accord with Raman vibrations analyzed by other researchers [12]. The spectra provide the evidence of scheelite structure for both products [12].

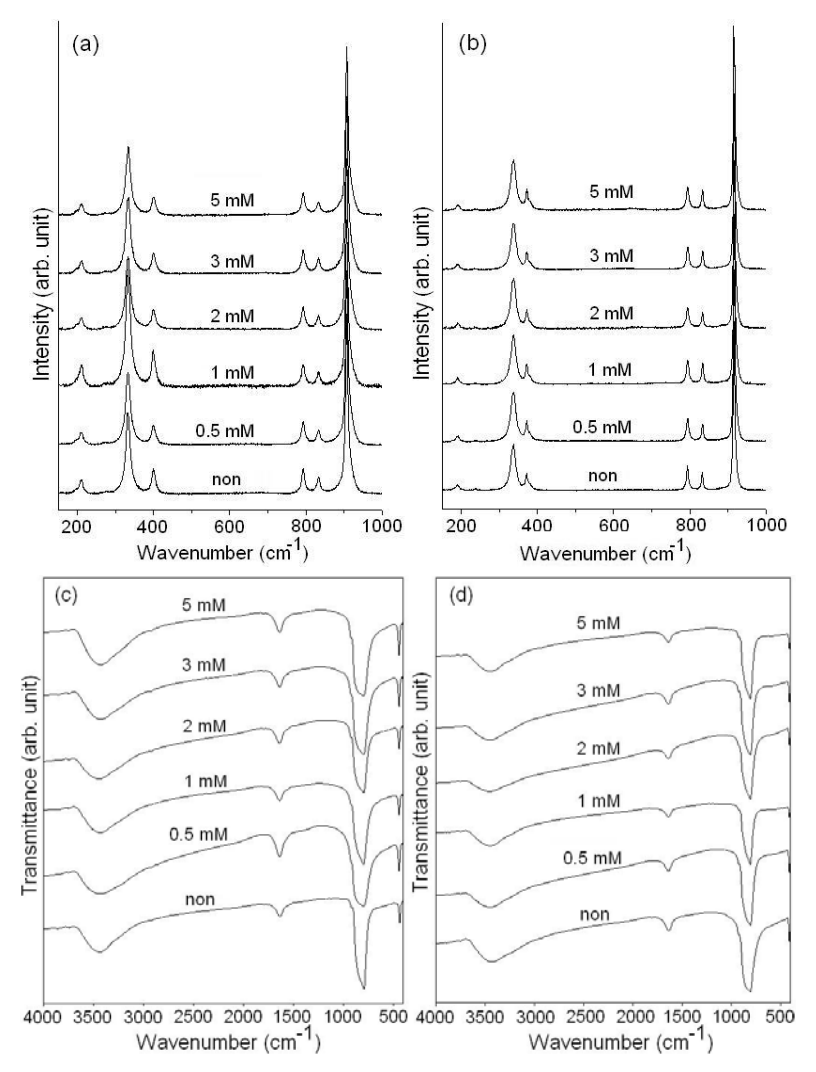


Fig. 2. Raman and FTIR spectra of (a, c) CaWO₄ and (b, d) SrWO₄ prepared with different moles of CTAB, respectively.

FTIR spectra shown in Figs. 2c and 2d were analyzed with a transmittance mode. For T_d symmetry, $v_3(F_2)$ and $v_4(F_2)$ are IR active and correspond to stretching and bending modes, respectively [14,15]. The spectra show a band of W-O stretching vibration in $[WO_4]^{2^-}$ tetrahedrons [3,14,15] at 793 and 807 cm⁻¹ for CaWO₄ and SrWO₄, respectively. They are the internal modes specified as $v_3(F_2)$ antisymmetric stretching vibrations [14,15]. Other weak W-O bending bands were detected at 438 and 410 cm⁻¹ for CaWO₄ and SrWO₄, respectively. O-H stretching and bending vibrations of residual water in CaWO₄ were detected at 3,435 and 1,635 cm⁻¹, and in SrWO₄ were at 3,442 and 1,637 cm⁻¹, respectively.

Fig. 3 shows SEM images of CaWO₄ and SrWO₄ composing of microsized particles with different morphologies. For CaWO₄ in a CTAB-free solution, it composes of nano-scale particles clustering together in microspheres, shown in Fig.

3a. In the solution containing 0.5 mM CTAB, the spheres were cleft into two parts; peach-like particles with the notches, shown in Fig. 3b. Subsequently, the peach-like particles were transformed into dumb-bells (Fig. 3c) and bundles (Fig. 3d) in the solutions containing 2 and 5 mM CTAB, respectively. The CTAB (cationic surfactant) functioned as a template or shaped director. When Na₂WO₄.2H₂O was mixed with CTAB, $[WO_4]^{2-}$ and the cations formed complex molecules. Subsequently, Ca(NO₃)₂.4H₂O was added in the mixture. The CTAB cations were replaced by Ca²⁺ ions to produce CaWO₄ by a microwave irradiation. During the preparation, vibrating electric field of a microwave applied a force on electric charged particles. Vibrations of the reactants have the influence on the proceeded reaction effectively. Once the CaWO₄ nuclei (very fine particles) formed, their growth could relate to the interaction between oriented CTAB chains and the nuclei. A uniform and ordered long chain structured CTAB adsorbed on the nucleus surfaces which led to the nucleus growth along the longitudinal direction [16]. There was some growth in the normal direction as well, but its rate was the slowest. The influence of the shaped director was increased with the increase of the CTAB moles. The spherical particles in the CTABfree solution were transformed step by step into bundles in the solution containing 5 mM CTAB. Some of the bundles were broken due to the microwave vibration frequency. For SrWO₄ in a CTAB-free solution, the products were the peach-like particles with the notches, as shown in Fig. 3e. When CTAB was added in the solution, the produced particles grew along the longitudinal direction. The products composed of a number of dumb-bells in the solutions containing 1 and 2 mM CTAB (Figs. 3f and 3g), and bundles in the 3 and 5 mM CTAB solutions (Figs. 3h and 3i). The cationic surfactant also had the same function as the above explanation.

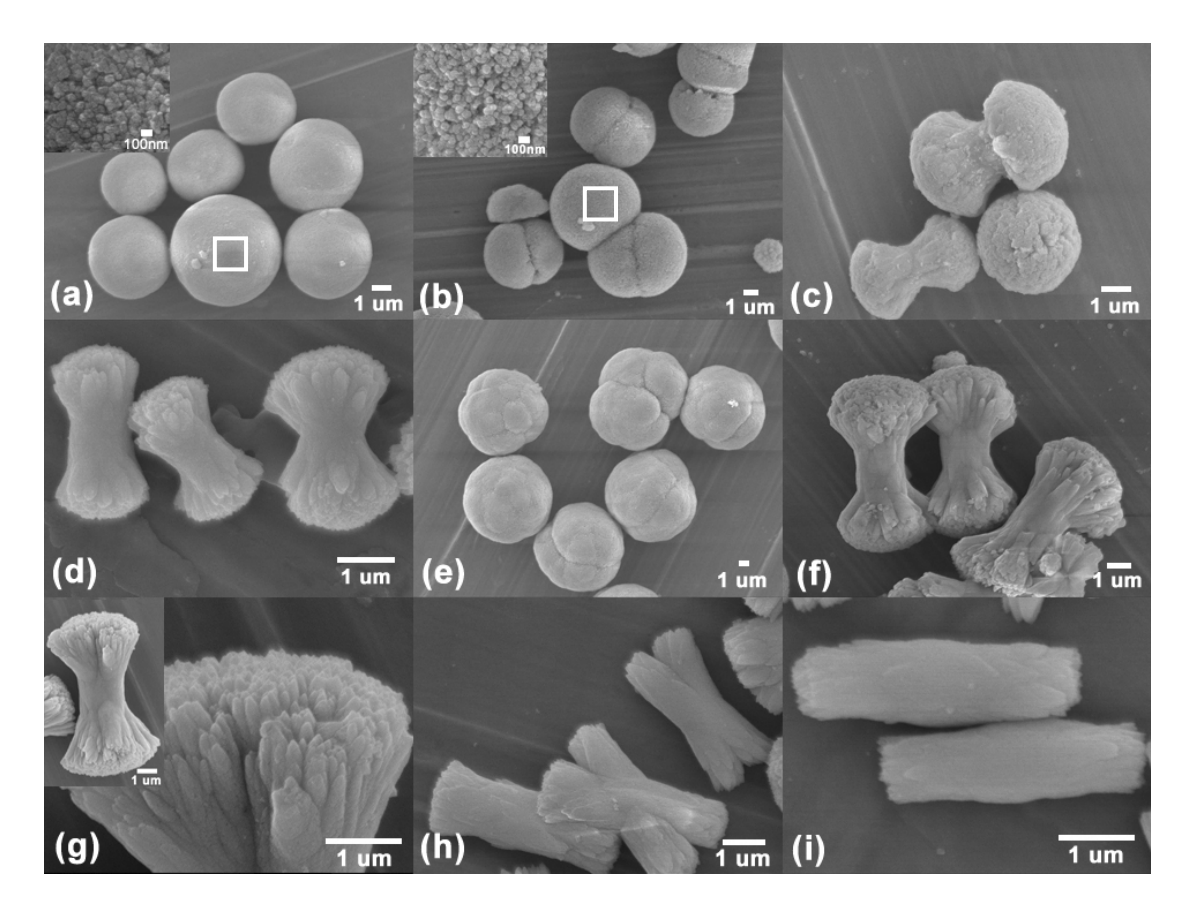


Fig. 3. SEM images of CaWO₄ prepared in (a) the CTAB-free solution, and (b-d) the solutions of 0.5, 2 and 5 mM CTAB, and of SrWO₄ prepared in (e) the CTAB-free solution, and (f-i) the solutions of 1, 2, 3 and 5 mM CTAB, respectively. The superimposed images at the upper lefts of the images (a) and (b) showed the closer view of the white rectangle areas of the corresponding images.

The structures of the produced particles were also investigated with TEM and SAED. In Fig. 4, the TEM images show CaWO₄ and SrWO₄ the shape of dumb-bell prepared in the 3 and 1 mM CTAB solution (Figs. 4a and 4d), respectively. The interpretations of the SAED patterns at the markers in the corresponding TEM images are shown in Figs. 4b and 4e, respectively [11,17]. These patterns show that each of product particles composes of single crystal. The calculated angles between any pair of the directions and the interplanar spaces determined from (hkl) are in accord with those of the diffraction patterns on their films. Calculated zone axes [11,17] are respectively in [041] and $[\overline{432}]$ directions parallel or nearly parallel to the electron beams. The patterns for CaWO₄ and SrWO₄ were simulated [18] using the corresponding directions as zone axes and are shown in Figs. 4c and 4f,

respectively. The patterns are symmetric and systematic, and are in good accord with those of the interpretations.

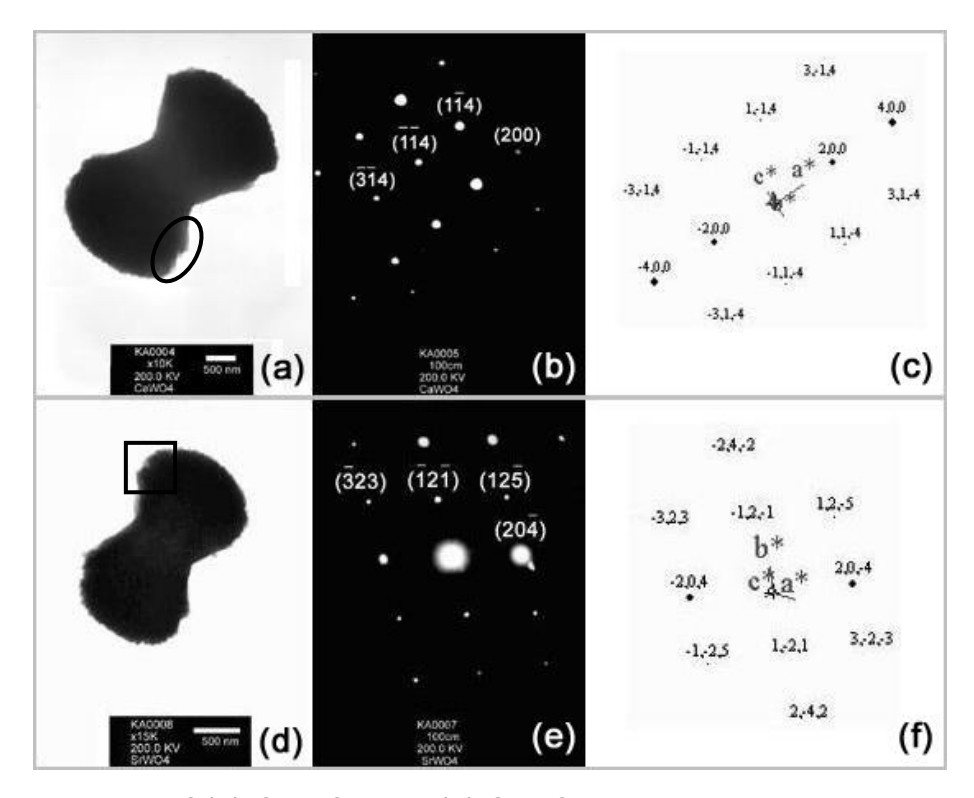


Fig. 4. TEM images of (a) CaWO₄ and (d) SrWO₄ particles prepared in 3 and 1 mM CTAB solutions, respectively. The interpreted SAED patterns were observed at the marked areas of ellipse (b) and square (e) in the TEM images. The schematic drawings of the corresponding SAED patterns are shown in (c) and (f).

PL spectra with different excitation wavelengths of 280 nm for CaWO₄ and 245 nm for SrWO₄ are shown in Fig. 5. They show the intrinsic peaks with their surrounding shoulders. The intrinsic peaks are considered to be from the $^1T_2 \rightarrow ^1A_1$ transition of electrons within [WO₄]²⁻ anions [19-21], which can be treated as excitons [21]. The shoulders are from some defects and/or impurities, and interpreted as extrinsic transitions [21]. PL intensity is controlled by the number of charged transfers. For the present analysis, the emission peaks are in the spectral region at 428-434 nm for CaWO₄, and 447-451 nm for SrWO₄. For most PL studies, their blue emissions were at 440 nm for CaWO₄, and 460 nm for SrWO₄ [5,22,23]. Comparing to the corresponding materials, the present emission peaks are blue-shift caused by the quantum-sized effect [24]. PL intensities are increased with the increase of the CTAB moles. They are the highest for the bundle-shaped CaWO₄ and SrWO₄ (5 mM

CTAB solutions). Shape and size of the crystals can also play a role in their emission peaks.

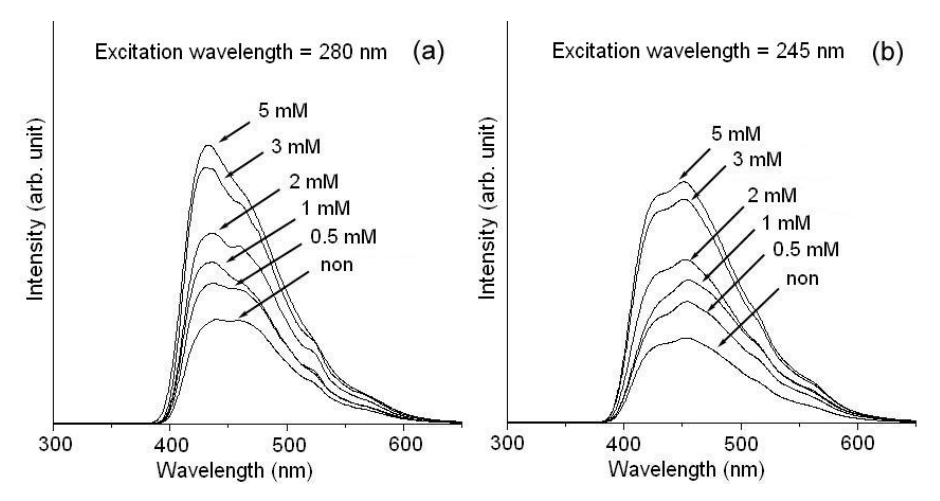


Fig. 5. PL spectra of (a) CaWO₄ and (b) SrWO₄ prepared with different moles of CTAB.

Conclusions

CaWO₄ and SrWO₄ were successfully synthesized with a cyclic microwave irradiation. The metal tungstates composed of nanosized particles in clusters with different shapes and sizes influenced by CTAB. They provided the evidence of scheelite structure with W-O stretching vibration in [WO₄]²⁻ tetrahedrons at 793 and 807 cm⁻¹ for CaWO₄ and SrWO₄, respectively. The PL emission peaks are in the spectral region at 428-434 nm for CaWO₄, and 447-451 nm for SrWO₄.

References

- [1] V.N. Kolobanov, I.A. Kamenskikh, V.V. Mikhailin, I.N. Shpinkov, D.A. Spassky, B.I. Zadneprovsky, L.I. Potkin, G. Zimmerer, Nuclear Instrum. Method. Phys. Res. A 486 (2002) 496.
- [2] Z.C. Ling, H.R. Xia, D.G. Ran, F.Q. Liu, S.Q. Sun, J.D. Fan, H.J. Zhang, J.Y. Wang, L.L. Yu, Chem. Phys. Lett. 426 (2006) 85.
- [3] G. Zhang, R. Jia, Q. Wu, Mater. Sci. Engin. B 128 (2006) 254.

- [4] S.H. Yoon, D.W. Kim, S.Y. Cho, K.S. Hong, J. Europ. Ceram. Soc. 26 (2006) 2051.
- [5] R. Zhai, H. Wang, H. Yan, M. Yoshimura, J. Cryst. Growth 289 (2006) 647.
- [6] T.T. Basiev, A.A. Sobol, Y.K. Voronko, P.G. Zverev, Optic. Mater. 15 (2000) 205.
- [7] L. Sun, Q. Guo, X. Wu, S. Luo, W. Pan, K. Huang, J. Lu, L. Ren, M. Cao, C. Hu, J. Phys. Chem. C. 111 (2007) 532.
- [8] V. Thangadurai, C. Knittlmayer, W. Weppner, Mater. Sci. Engin. B 106 (2004) 228.
- [9] A. Sen, P. Pramanik, J. Europ. Ceram. Soc. 21 (2001) 745.
- [10] Powder Diffract. File, JCPDS Internat. Centre Diffract. Data, PA 19073-3273, U.S.A., (2001).
- [11] T. Thongtem, A. Phuruangrat, S. Thongtem, Mater. Lett. 61 (2007) 3235.
- [12] S.P.S. Porto, J.F. Scott, Phys. Rev. 157 (1967) 716.
- [13] A. Golubović, R. Gajić, Z. Dohčević-Mitrović, S. Nikolić, J. Alloys Comp. 415 (2006) 16.
- [14] A.P. de Azevedo Marques, D.M.A. de Melo, C.A. Paskocimas, P. S. Pizani, M.R. Joya, E.R. Leite, E. Longo, J. Solid State Chem. 179 (2006) 671.
- [15] J.A. Gadsden, Infrar. Spectr. Miner. Related Inorg. Comp. Butterworths, (1975).
- [16] T. Saraidarov, R. Reisfeld, A. Sashchiuk, E. Lifshitz, Physica E 37 (2007) 173.
- [17] T. Thongtem, A. Phuruangrat, S. Thongtem, Mater. Lett. 62 (2008) 454.
- [18] C. Boudias, D. Monceau, CaRlne Crystallography 3.1, 17 rue du Moulin du Roy, F-60300 Senlis, France, (1989-1998).
- [19] Y. Zhang, N.A.W. Holzwarth, R.T. Williams, Phys. Rev. B 57 (1998) 12 738.
- [20] M.J. Treadaway, R.C. Powell, J. Chem. Phys. 61 (1974) 4003.
- [21] V.B. Mikhailik, I.K. Bailiff, H. Kraus, P.A. Rodnyi, J. Ninkovic, Radiat. Measur. 38 (2004) 585.
- [22] Z. Lou, M. Cocivera, Mater. Res. Bull. 37 (2002) 1573.
- [23] W.S. Cho, M. Yashima, M. Kakihana, A. Kudo, T. Sakata, M. Yoshimura, Appl. Phys. Lett. 68 (1996) 137.
- [24] R. Jia, Q. Wu, G. Zhang, Y. Ding, J. Mater. Sci. 42 (2007) 4887.

Characterization of MeWO₄ (Me = Ba, Sr and Ca) nanocrystallines prepared by sonochemical method

Abstract

Metal tungstates (MeWO₄, Me = Ba, Sr and Ca) were successfully prepared using the corresponding Me(NO₃)₂.2H₂O and Na₂WO₄.2H₂O in ethylene glycol by the 5 h sonochemical process. The tungstate phases with scheelite structure were detected with X-ray diffraction (XRD) and selected area electron diffraction (SAED). Their calculated lattice parameters are in accord with those of the JCPDS cards. Transmission electron microscopy (TEM) revealed the presence of nanoparticles composing the products. Their average sizes are 42.0 ± 10.4 , 18.5 ± 5.1 and 13.1 ± 3.3 nm for Me = Ba, Sr and Ca, respectively. Interplanar spaces of the crystals were also characterized with high resolution TEM (HRTEM). Their crystallographic planes are aligned in systematic array. Six different vibration wavenumbers were detected using Raman spectrometer and are specified as $v_1(A_g)$, $v_3(B_g)$, $v_4(B_g)$, $v_2(A_g)$ and free rotation. Fourier Transform Infrared (FTIR) spectra provided the evidence of scheelite structure with W-O anti-symmetric stretching vibration of [WO₄]²⁻ tetrahedrons at 786-883 cm⁻¹. Photoluminescence emission of the products was detected over the range 384-416 nm.

Keywords: Sonochemical method; BaWO₄; SrWO₄; CaWO₄; Nanocrystallines

Introduction

Recently, the research on nanocrystallines has been increasingly progressive due to their novel properties. Among them, MeWO₄ (Me = Ba, Sr and Ca) with scheelite structure are such the materials [1,2]. There are W ions in tetrahedrons composing of O ions. Me ions are surrounded with eight O ions [3]. The properties of MeWO₄ nanocrystallines are influenced by the chemical composition, structure, phase and morphologies. The tungstates are very useful in a variety of applications, such as scintillators [2,3], stimulated Raman scattering [1], optoelectronic devices [4] and catalysts [5]. They were prepared by a variety of methods, such as a simple template-free precipitation technique [1], spray pyrolysis [2], microwave-assisted

synthesis [5], chemical solution method [6], a facile microemulsion-mediated hydrothermal process [7] and electrochemical method [8].

Currently, nano-structured materials have been found to exhibit anomalous properties which are totally different from their bulks [9]. The physical and chemical properties are influenced by the particle sizes, which were caused by quantum confinement effects [10]. For such the particles, percents of surface area per unit volume are very large. Their optical absorption wavelengths exhibited blue-shift comparing with the corresponding bulk materials [11]. Due to these favorable properties, the nano-particles are being extensively studied for used in a variety of applications.

Sonochemical process has very attractive attention used for preparing materials. It can lead to more uniform distribution of nanoparticles, smaller sizes, slightly higher surface area and better thermal stability and phase purity than that achieved by the conventional method [12]. When ultrasonic radiation is supplied to chemical solutions, their molecules vibrate accordingly and heat develops. Vibration of molecules can solve the problems of concentration and temperature gradients. The radiation has the influence on the reaction to proceed with efficiency and shorter time. Subsequently, pure products were produced.

Ethylene glycol (heat capacity at 25 °C = 150.4 J.mol⁻¹.K⁻¹ [13]) is able to assist in forming the complex and stabilizing the nanoparticles. It promotes the particles to exist as non-cluster [14]. Temperature rising develops in ethylene glycol is two times slower than that in water (heat capacity at 25 °C = 75.4 J.mol⁻¹.K⁻¹ [13]). Therefore, it is good choice for using ethylene glycol as the solvent for the synthesis of nanoparticles.

The purpose of the research is to prepare $MeWO_4$ (Me = Ba, Sr and Ca) nanocrystallines with novel properties in ethylene glycol by the sonochemical method. The reaction proceeded in an open system at atmospheric pressure. No other additives were used. The process is very simple, attractive and novel for preparing pure products.

Experiment

Each of 5 mM $Me(NO_3)_2.2H_2O$ (Me = Ba, Sr and Ca) and $Na_2WO_4.2H_2O$ was dissolved in 30 ml ethylene glycol. The reactions proceeded for 5 h by the application of powerful ultrasonic radiation (35 kHz) on according to the following.

The final products were washed with water and ethanol, dried at 70 $^{\circ}$ C for 12 h, and intensively characterized.

Results and Discussion

Crystallographic planes on XRD spectra (Fig 1) were indexed using Bragg's law for diffraction. The planes correspond to MeWO₄ (Me = Ba, Sr and Ca) (reference codes : 43-0646, 85-0587 and 41-1431) [15]. Their strongest intensity peaks diffracted from the same plane specified as (112). They have scheelite structure with tetragonal crystal system [1-3,6,16,17] and have I4₁/a or C_{4h}^6 space-group symmetry [2,15,16]. Calculated lattice parameters [18] for BaWO₄ (a = b = 0.5618, c = 1.2734 nm), SrWO₄ (a = b = 0.5415, c = 1.1962 nm) and CaWO₄ (a = b = 0.5248, c = 1.1394 nm) are very close to those of the corresponding JCPDS cards [15], and have the influence on the spaces between crystallographic planes. No other characteristic peaks of impurities were detected showing that the products are pure phase.

Raman vibrations of MeWO₄ are divided into two groups, the internal and external modes [19]. The internal mode is the W-O vibration within $[WO_4]^{2^-}$ tetrahedral units with immobile mass centers. The external one or lattice phonon corresponds to the vibration of Me^{2^+} cations relative to the rigid tetrahedral units. In free space, $[WO_4]^{2^-}$ tetrahedrons have T_d -symmetry [17,19]. Their vibrations compose of four internal modes $(v_1(A_1), v_2(E), v_3(F_2))$ and $v_4(F_2)$, one free rotation $(v_{f.r.}(F_1))$, and one translation (F_2) [19]. In lattice space, they have S_4 -symmetry. All degenerative vibrations are split [17,19] due to the crystal field effect and Davydov splitting [19]. By using group-theory calculation, there are 26 different modes for tetragonal scheelite primitive cell (wavevector, k = 0), three for A_g and B_u , and five for A_u , A_g ,

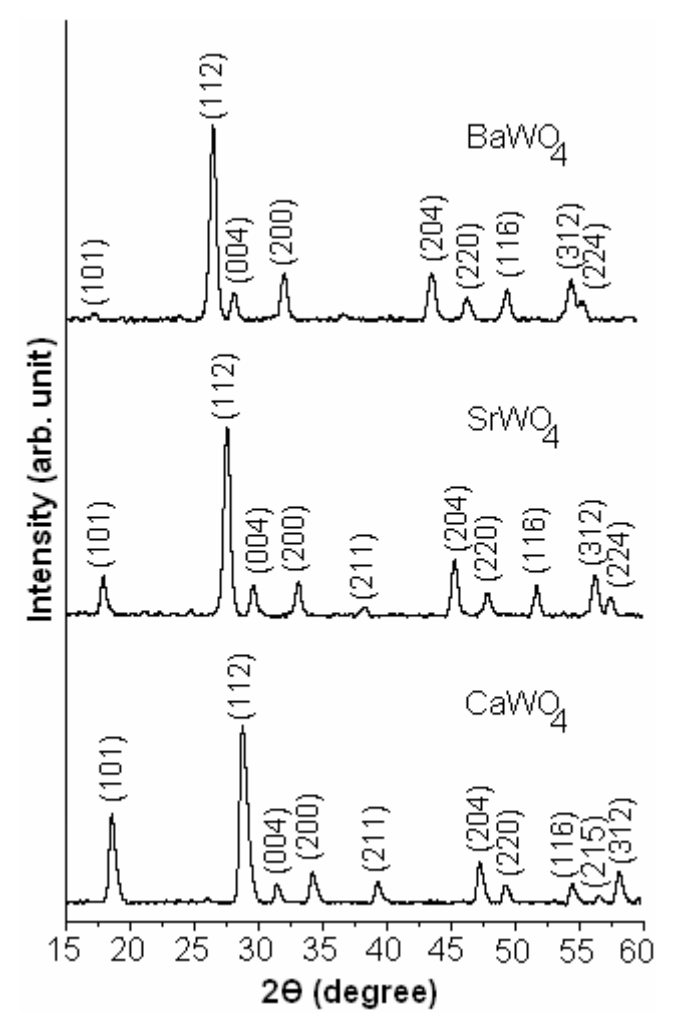


Fig 1. XRD spectra of BaWO₄, SrWO₄ and CaWO₄ prepared by sonochemical method.

Six different modes $(v_1(A_g), v_3(B_g), v_4(B_g), v_4(B_g), v_2(A_g))$ and free rotation) were detected on Raman spectra (Fig 2a) at 921, 826, 791, 345, 332 and 191 cm⁻¹ for BaWO₄, 922, 838, 799, 372, 337 and 190 cm⁻¹ for SrWO₄, and 913, 838, 798, 401, 337 and 211 cm⁻¹ for CaWO₄, respectively. Each of the modes is in accord with Raman vibrations analyzed by other researchers [17,19]. The spectra of the three products provide the evidence of scheelite structure [17,19]. Comparing to Ar laser (λ = 514.5 nm), a great deal of energy was lost during the inelastic scattering process. In addition, FTIR spectra (Fig 2b) were analyzed using a transmittance mode. For T_d-symmetry, vibration frequencies of [WO₄]²⁻ tetrahedrons are $v_1(A_1)$, $v_2(E)$, $v_3(F_2)$ and $v_4(F_2)$ [20]. In lattice space, their site symmetries become S₄. The correlation of the two point groups (T_d \rightarrow S₄) is as follows: A₁ \rightarrow A, E \rightarrow A + B and F₂ \rightarrow B + E. Only bands corresponding to v_2 , v_3 and v_4 were detected [20]. Main transmittance bands

 (v_3) specified as W-O anti-symmetric stretching vibration of $[WO_4]^{2^-}$ tetrahedrons in lattice space [21] were detected at 786-883 cm⁻¹. Sometimes they split into two bands, sometimes they do not [20,22,23]. For present result, it appears as the strong broad band. The v_4 splits into two bands at the wavenumbers of less than 400 cm⁻¹ [20]. Additional weak peak of W-O bending band was also detected at 447 cm⁻¹ for CaWO₄. It was specified as v_2 band [20,24]. The present analysis is in accord with other results [22,23].

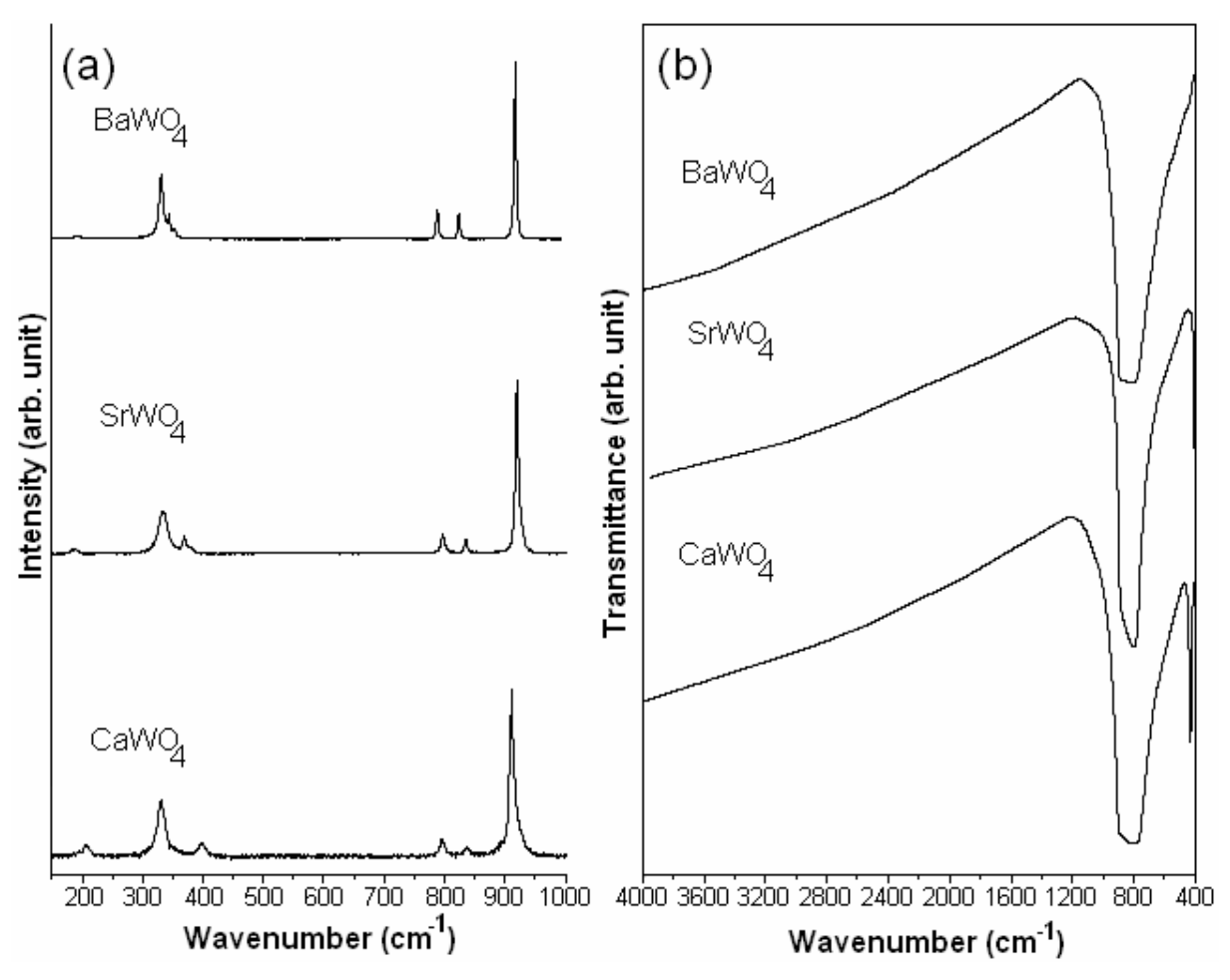


Fig 2. (a) Raman and (b) FTIR spectra of BaWO₄, SrWO₄ and CaWO₄ prepared by sonochemical method.

For the resolution of 0.10 nm, TEM images (Fig 3) show that the three products compose of a number of dispersed nanosized particles with round shape. Among them, the sizes ranging from the biggest to the smallest are BaWO₄, SrWO₄ and CaWO₄, respectively. SAED patterns (Fig 3) are diffuse showing that the products compose of nanosized particles. Each of them is polycrystal. They were also caused

by a number of single crystals with different orientations. The patterns appear as concentric rings, due to the diffraction of electrons through the nanosized particles. The rings were interpreted [25,26], and specified as (112), (200), (114), (204), (220), (116) and (224) planes for BaWO₄, (101), (112), (004), (200), (211), (204), (220), (116) and (312) planes for SrWO₄, and (101), (112), (004), (200), (211), (204), (220), (116) and (312) planes for CaWO₄ [15]. The (112) plane has the strongest intensity composing the SAED patterns. Their strongest intensities are in accord with those of the corresponding XRD spectra. Lattice planes (Fig 4) show that atoms are uniformly arranged in systematic array. The detected spaces correspond to (112), (112) and (101) planes for BaWO₄, SrWO₄ and CaWO₄, respectively. The particle sizes (Fig 5) were determined [27]. The distributions are very close to the normal curves. They are in the ranges 7.5-75, 1-35 and 2-24 nm with the average of 42.0 ± 10.4 , 18.5 ± 5.1 and 13.1 ± 3.3 nm for BaWO₄, SrWO₄ and CaWO₄, respectively. Their shapes and sizes have the influence on the photoluminescent properties as well.

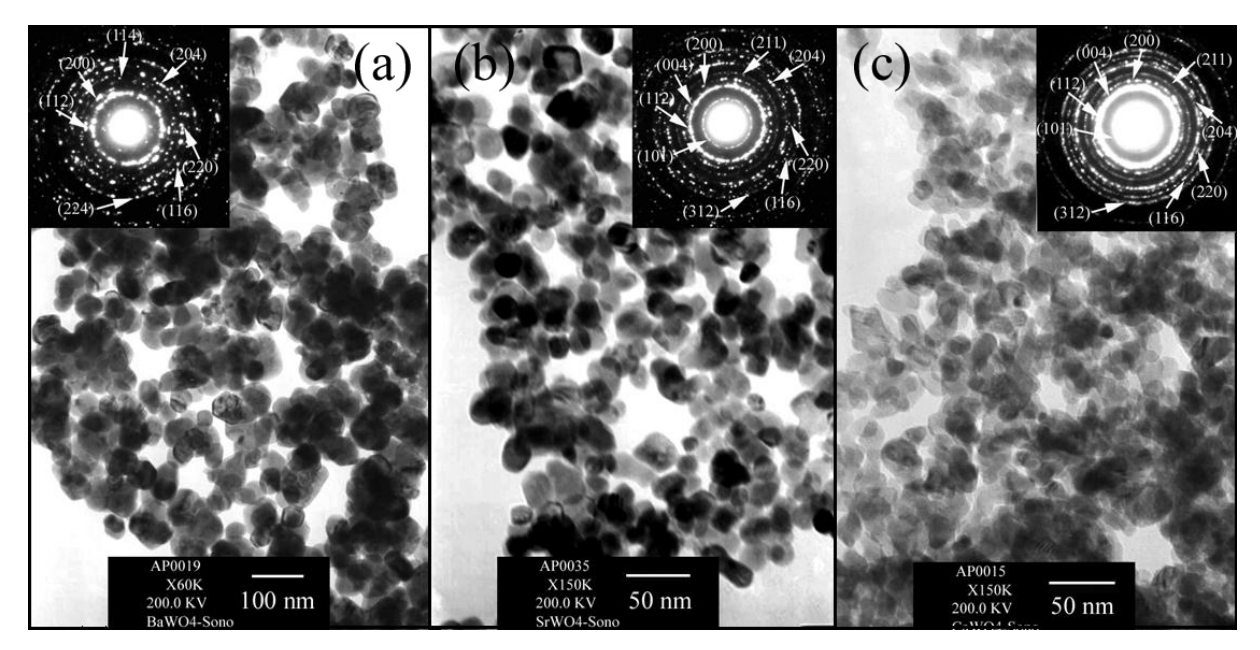


Fig 3. TEM images and SAED patterns of (a) BaWO₄, (b) SrWO₄ and (c) CaWO₄.

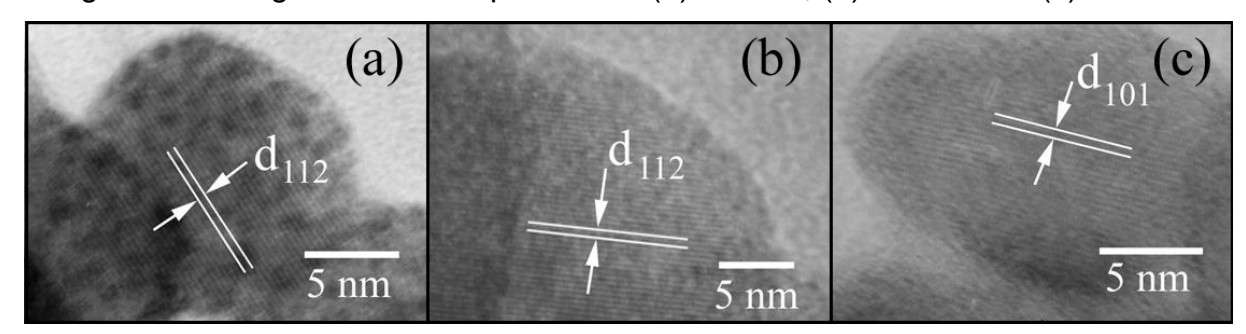


Fig 4. HRTEM images of (a) BaWO₄, (b) SrWO₄ and (c) CaWO₄.

The crystal-field splitting and hybridization of the molecular orbitals of $[WO_4]^{2-1}$ tetrahedrons [16] are shown in Fig 6. The W $5d(t_2)$ and W 5d(e) orbitals are hybridized with the O $2p(\sigma)$ and O $2p(\pi)$ ligand orbitals to form $[WO_4]^{2-1}$ tetrahedrons. The four ligand $p(\sigma)$ orbitals are compatible with the tetrahedral representation for a_1 and a_2 symmetries and the eight ligand a_2 orbitals are for a_3 are for a_4 and a_4 symmetries and the eight ligand a_4 orbitals are for a_4 and a_4 symmetries. The top occupied state has a_4 symmetry formed from O a_4 orbitals. The lowest unoccupied state has e symmetry formed from a combination of the W a_4 orbitals to give anti-bonding (*). The hybridization between the W a_4 and O a_4 orbitals is specified as covalent bonding between the ions. For ground state system, all one-electron states below band gap are filled to give a many-electron a_4 state. At the lowest excited state, there are one hole in a_4 (primarily O a_4) state and one electron in e (primarily W a_4) state which give rise to many-electron a_4 and a_4 or a_4 states. Among them, only a_4 transition is electric dipole allow [16,28].

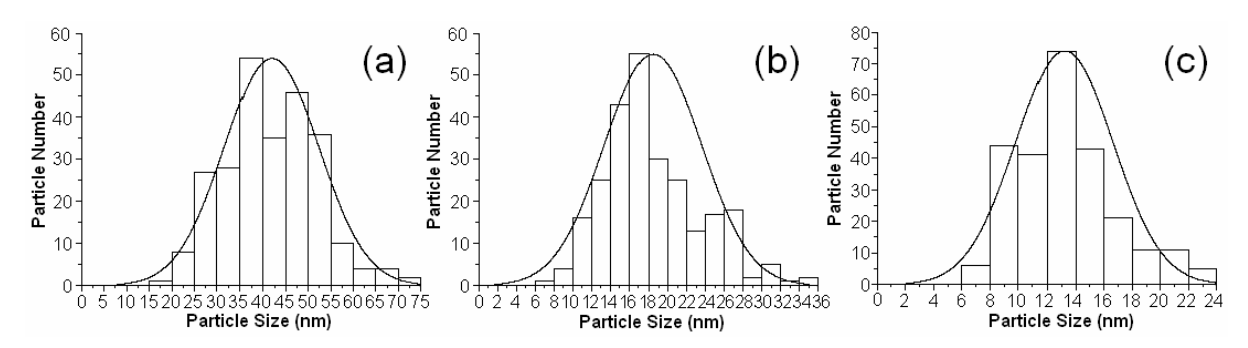


Fig 5. Particle size distributions of (a) BaWO₄, (b) SrWO₄ and (c) CaWO₄.

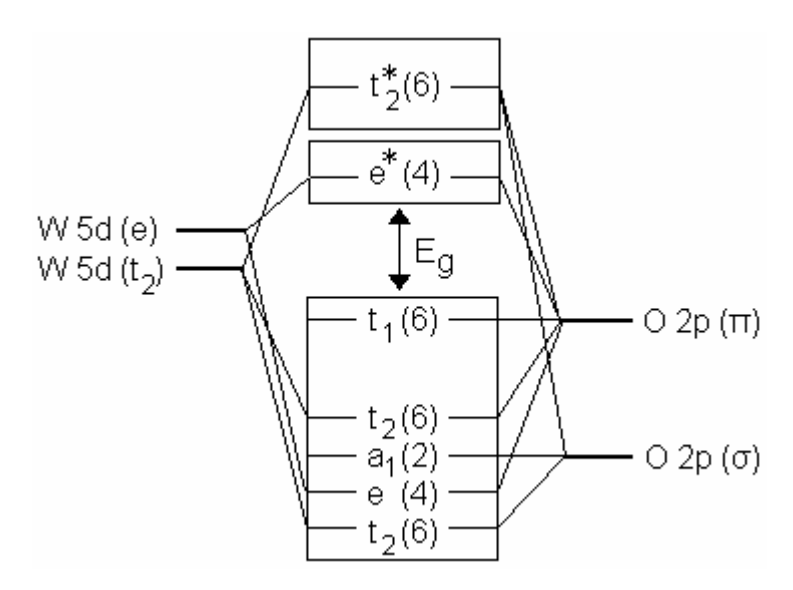


Fig 6. Diagram of the crystal-field splitting and hybridization of the molecular orbitals of $[WO_4]^{2-}$ tetrahedrons. $[E_g = Energy band gap, * = Anti-bonding (Unoccupied) states, Degeneracy of each cluster state is specified in parentheses.]$

By respective using of 344, 270 and 214 nm exciting wavelengths for BaWO₄, SrWO₄ and CaWO₄, photoluminescent (PL) spectra (Fig 7) have the narrow central peaks with their surrounding shoulders. The central (intrinsic) peaks are considered to be from the ${}^1T_2 \rightarrow {}^1A_1$ transition of electrons within [WO₄]²⁻ anions [16,28,29]. The transition can be treated as an exciton [29]. The shoulders are from some defects and impurities, and are specified as extrinsic transition [29]. PL intensity is controlled by the number of charged transfers. For the present analysis, the emission peaks are in the spectral region at 384-416 nm. The results are in the same range as others [22,29,30]. Comparing to the corresponding bulks, their emission peaks are blue-shift [22] caused by the quantum-sized effect [10].

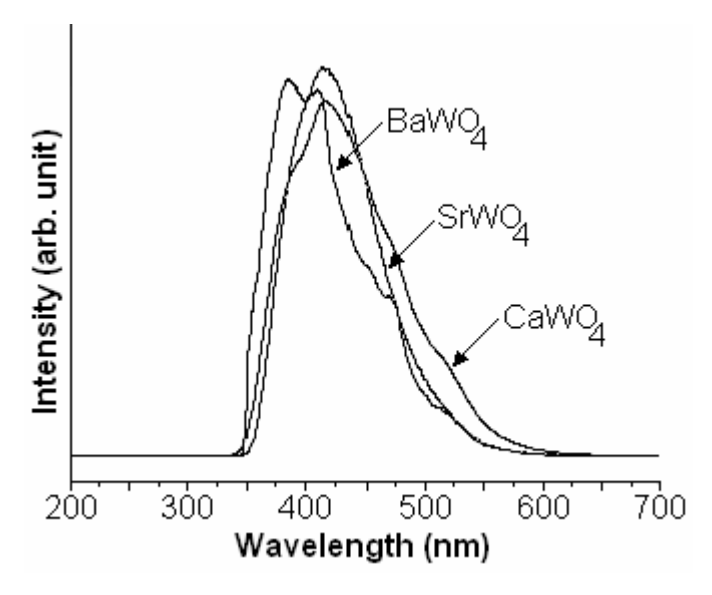


Fig 7. PL spectra of BaWO₄, SrWO₄ and CaWO₄.

Conclusions

BaWO₄, SrWO₄ and CaWO₄ were successfully prepared by sonochemical method. Each of them is pure phase, and composes of dispersed nanocrystallines. They are in the ranges 7.5-75, 1-35 and 2-24 nm for BaWO₄, SrWO₄ and CaWO₄, respectively. Their atoms are uniformly arranged in lattice array. The evidence of scheelite structured products was provided. Main transmittance bands specified as W-O antisymmetric stretching vibration were detected at 786-883 cm⁻¹. Their emission peaks are due to the $^{1}T_{2} \rightarrow ^{1}A_{1}$ electronic transition of [WO₄]²⁻ tetrahedrons in the spectral region at 384-416 nm. They are blue-shift relative to the corresponding bulks.

References

- [1] X. Wang, H. Xu, H. Wang, H. Yan, J. Crys. Growth 284 (2005) 254.
- [2] Z. Lou, M. Cocivera, Mater. Res. Bull. 37 (2002) 1573.
- [3] A. Golubović, R. Gajić, Z. Dohčević-Mitrović, S. Nikolić, J. Alloys Comp. 415 (2006) 16.
- [4] C. Zhang, E. Shen, E. Wang, Z. Kang, L. Gao, C. Hu, L. Xu, Mater. Chem. Phys. 96 (2006) 240.

- [5] J.H. Ryu, J.W. Yoon, C.S. Lim, W.C. Oh, K.B. Shim, Ceram. Internat. 31 (2005) 883.
- [6] M.A.M.A. Maurera, A.G. Souza, L.E.B. Soledade, F.M. Pontes, E. Longo, E.R. Leite, J.A. Varela, Mater. Lett. 58 (2004) 727.
- [7] L. Sun, M. Cao, Y. Wang, G. Sun, C. Hu, J. Crys. Growth 289 (2006) 231.
- [8] W.S. Cho, M. Yashima, M. Kakihana, A. Kudo, T. Sakata, M. Yoshimura, Appl. Phys. Lett. 68 (1996) 137.
- [9] A. Datta, A. Saha, A.K. Sinha, S.N. Bhattacharyya, S. Chatterjee, J. Photochem. Photobiol. B 78 (2005) 69.
- [10] N.M. Huang, C.S. Kan, P.S. Khiew, S. Radiman, J. Mater. Sci. 39 (2004) 2411.
- [11] J.R. Lakowicz, I. Gryczynski, Z. Gryczynski, C.J. Murphy, J. Phys. Chem. B 103 (1999) 7613.
- [12] A. Gedanken, Ultras. Sonochem. 11 (2004) 47.
- [13] J.Y. Huot, E. Battistel, R. Lumry, G. Villeneuve, J.F. Lavallee, A. Anusiem, C. Jolicoeur, J. Soln. Chem. 17 (1988) 601.
- [14] D. Chen, G. Shen, K. Tang, H. Zheng, Y. Qian, Mater. Res. Bull. 38 (2003) 1783.
- [15] Powder Diffract. File, JCPDS Internat. Centre Diffract. Data, PA 19073-3273, U.S.A., (2001).
- [16] Y. Zhang, N.A.W. Holzwarth, R.T. Williams, Phys. Rev. B 57 (1998) 12 738.
- [17] S.P.S. Porto, J.F. Scott, Phys. Rev. 157 (1967) 716.
- [18] T. Thongtem, A. Phuruangrat, S. Thongtem, Mater. Lett., 61 (2007) 3235.
- [19] T.T. Basiev, A.A. Sobol, Y.K. Voronko, P.G. Zverev, Optic. Mater. 15 (2000) 205.
- [20] G.M. Clark, W.P. Doyle, Spectrochim. Acta 22 (1966) 1441.
- [21] Z.C. Ling, H.R. Xia, D.G. Ran, F.Q. Liu, S.Q. Sun, J.D. Fan, H.J. Zhang, J.Y. Wang, L.L. Yu, Chem. Phys. Lett. 426 (2006) 85.
- [22] G. Zhang, R. Jia, Q. Wu, Mater. Sci. Engin. B 128 (2006) 254.
- [23] F.A. Miller, C.H. Wilkins, Anal. Chem. 24 (1952) 1253.
- [24] R.L. Frost, L. Duong, M. Weier, Spectrochim. Acta Part A 60 (2004) 1853.
- [25] T. Thongtem, S. Kaowphong, S. Thongtem, J. Mater. Sci. 42 (2007) 3923.
- [26] A. Phuruangrat, T. Thongtem, S. Thongtem, Mater. Lett., 61 (2007) 3805.
- [27] Scion Image, Scion Corp., 82 Worman's Mill Ct., Suite H, Frederick, MD 21701 (1997-2005).
- [28] M.J. Treadaway, R.C. Powell, J. Chem. Phys. 61 (1974) 4003.

[29] V.B. Mikhailik, I.K. Bailiff, H. Kraus, P.A. Rodnyi, J. Ninkovic, Radiat. Measur. 38 (2004) 585.

[30] G. Zhou, M. Lü, Z. Xiu, S. Wang, H. Zhang, W. Zou, J. Crys. Growth 276 (2005) 116.

Characterization of PbS with different morphologies produced using a cyclic microwave radiation

Abstract

PbS was produced from different lead (Pb(CH₃COO)₂.H₂O, PbCl₂.2.5H₂O, Pb(NO₃)₂) and sulfur (CH₃CSNH₂, CH₅N₃S, NH₂CSNH₂) sources in propylene glycol using a cyclic microwave radiation at different powers and prolonged times. PbS (cubic) was detected using X-Ray Diffraction (XRD) and Selected Area Electron Diffraction (SAED) techniques. The interpreted and simulated patterns are in good accord. Raman spectrometer revealed the presence of vibrations at 138, 273 and 439 cm⁻¹. Different morphologies (nano-sized particles, hexapods, cubes, ferns and magic squares) were characterized using a Scanning Electron Microscope (SEM) and a Transmission Electron Microscope (TEM). The product morphologies were influenced by the starting agents, microwave powers and prolonged times.

Keywords: Cyclic microwave radiation; PbS; Nano-sized particles; Hexapods; Cubes; Ferns; Magic squares

Introduction

At present, luminescent materials with different morphologies have become increasingly important. One of them is PbS, which has a small band gap (0.41 eV) and a large exciton Bohr radius (18 nm) [1,2]. The sulfide with nanoparticles possesses the third order nonlinear optical property, which has the potential for using in optical devices [3]. PbS nanocrystals (irregular nanoparticles, star-shaped dendrites, truncated nanocubes and nanocubes) showed an emission spectra at the same wavelength of 632 nm although their morphologies are different. Nanocubes with the best crystals contain very low defect concentration. The intensity is the highest, compared with other nanocrystals. But for irregular nanoparticles, the intensity is the lowest. The emission properties are influenced by several parameters, such as shapes, sizes, size distributions and defects [4]. In addition, absorption UV spectra of PbS nanocrystals the shapes of nanorods, nanobelts, nanodendrites and

nanovelvet-flowers were very large blue-shift relative to its bulk due to the quantum size effect [3]. The product with different morphologies was produced using a variety of methods such as dendritic PbS nanostructures by ultrasonic method [5], hollow nanospheres by sonochemical method [6], nanoparticles by a simple polyol route [7], cross-shaped PbS nanostructures by a surfactant-assisted reflux process [8] and nanocrystals in ethanol by a microwave heating synthesis [9]. Microwave radiation is very attractive used for preparing materials. It can rapidly lead to very high temperatures which have an influence on the reaction rates. When microwave is supplied to solutions, one or more of the components is capable of coupling with the radiation. Vibrating electric field applied a force on charged particles which vibrated accordingly. It can lead to higher heating rate than that achieved by conventional method, and can solve the problems of temperature and concentration gradients. Subsequently, pure products were produced [10]. The present research is to investigate the role of lead and sulfur sources on the morphologies of PbS produced in propylene glycol using a cyclic microwave radiation without any further calcination.

Experiment

PbS with different morphologies was produced from 0.005 mol each of lead and sulfur sources (Table 1) in 30 ml propylene glycol using a cyclic microwave radiation at different powers and prolonged times. One cycle of 100 s prolonged time composes of 30 s radiation and 70 s non-radiation. Test temperatures for the present research are shown in Fig 1. They were increased with the increase in the microwave powers and prolonged times. The temperatures rapidly increased during the first 15 min. Their rates decreased afterwards. For 180 W, the temperature tended to be constant at 80 °C after 20 min test. At the conclusion of the test, the final products were washed with water and ethanol, and dried at 80 °C for 12 h. Then, they were characterized using an X-ray diffractometer (XRD) operated at 20 kV, 15 mA and using Cu K_{α} radiation in the 20 angular range of 15 - 60 deg, a transmission electron microscope (TEM) as well as the use of the selected area electron diffraction (SAED) technique operated at 200 kV, a scanning electron microscope (SEM) operated at 15 kV and a Raman spectrometer using 50 mW Ar Laser with λ = 514.5 nm at room temperature.

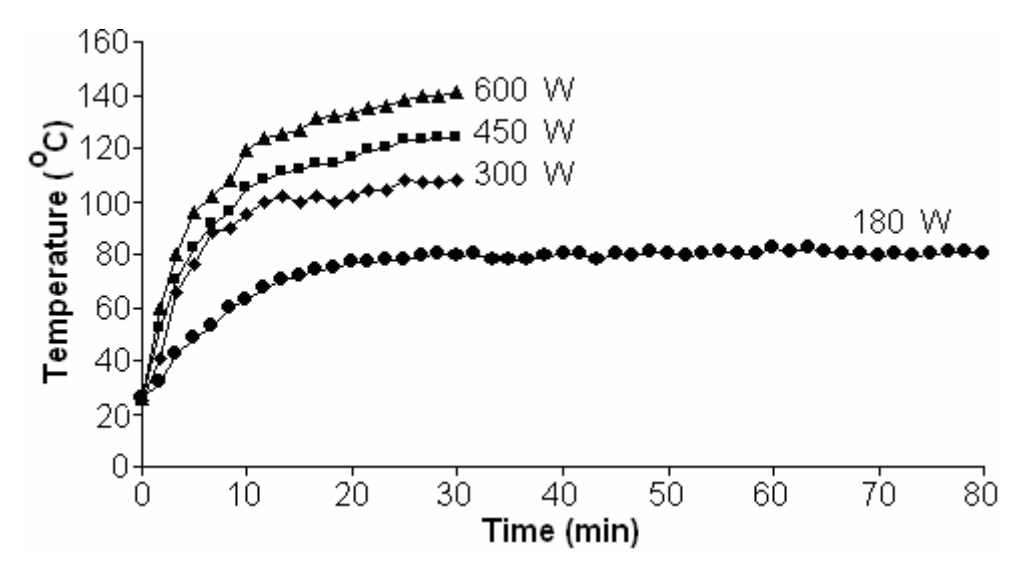


Fig 1. Test temperatures at different microwave powers and prolonged times.

Table 1. Lead and sulfur sources, product codes and the products morphologies.

Lead sources	Sulfur sources	Product	Product
		codes	morphologies
Pb(CH ₃ COO) ₂ .H ₂ O	CH₃CSNH₂	AA	Nano-sized particles
	CH_5N_3S	AC	Hexapods
	NH ₂ CSNH ₂	AT	Hexapods
PbCl ₂ .2.5H ₂ O	CH₃CSNH₂	CA	Cubes
	CH_5N_3S	CC	Nano-sized particles
	NH ₂ CSNH ₂	СТ	Nano-sized particles
Pb(NO ₃) ₂	CH₃CSNH₂	NA	Cubes
	CH_5N_3S	NC	Ferns
	NH ₂ CSNH ₂	NT	Magic squares

Results and Discussion

Crystallographic planes of XRD spectra (Figs 2 and 3) were indexed using Bragg's law for X-ray diffraction and compared with those of the JCPDS software (reference code: 05-0592) [11]. At 180 W for 30 min, the product is so less that it is not able to collect from the filter paper. For longer times (Fig 2a), higher powers (Fig 2b), and different lead and sulfur sources at 600 W for 15 min (Figs 3a-3c), the products were specified as cubic PbS with Fm-3m space group. Their intensities increased with the

increase in the prolonged times and microwave powers. These reflect the degree or extent of the crystals. For present analysis, well-crystallized PbS was successfully synthesized [12]. The products compose of a number of atoms aligning in a periodic lattice. The strongest intensity is at $2\theta = 30.08$ deg and diffracted from (200) plane of the crystalline products. No other impurities were detected although the products were produced using different conditions. XRD spectra were characterized over the 2θ angular range of 15 - 60 deg, which covers the main peaks with high intensities. The peaks with $2\theta > 60$ deg, such as (400) and (331), were off-scale and were not detected.

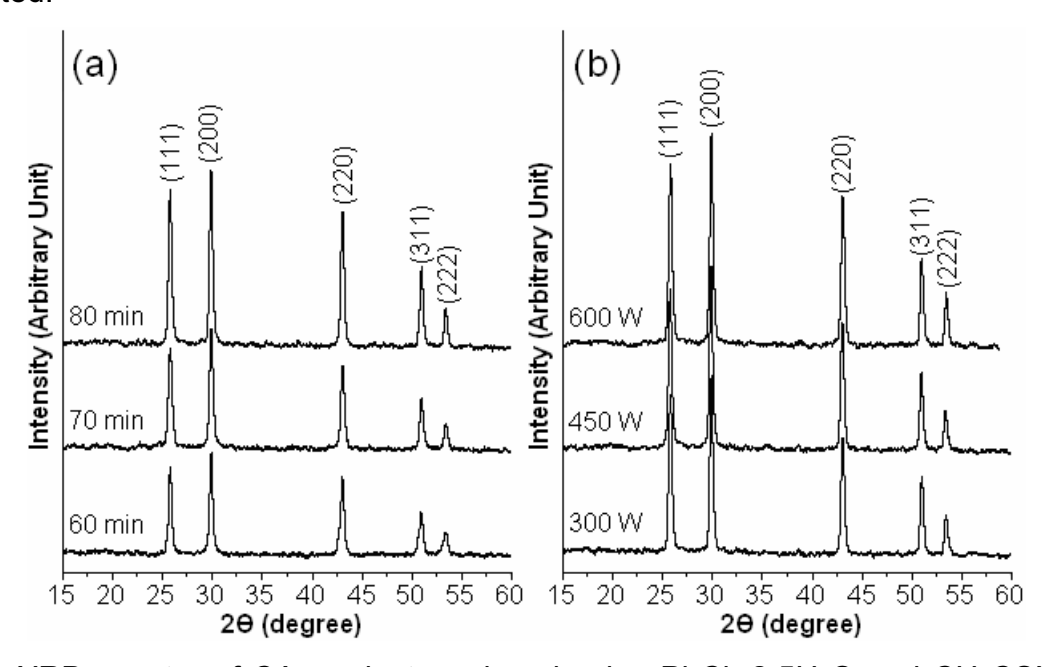


Fig 2. XRD spectra of CA product produced using PbCl₂.2.5H₂O and CH₃CSNH₂ at (a) 180 W microwave power for different prolonged times, and (b) different microwave powers for 15 min.

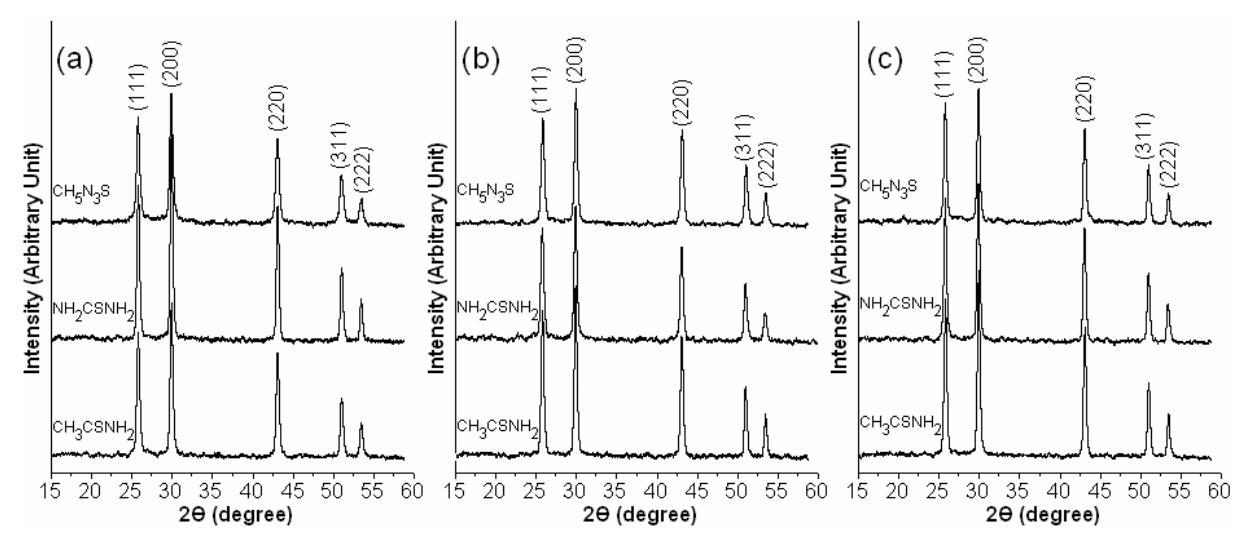


Fig 3. XRD spectra of PbS produced using (a) Pb(CH₃COO)₂.H₂O, (b) PbCl₂.2.5H₂O and (c) Pb(NO₃)₂ with different sulfur sources at 600 W microwave power for 15 min.

SEM and TEM images (Figs 4 and 5) show that the products were successfully produced in a variety of shapes and sizes which are summarized in Table 1. The AC and AT products (Figs 4a and 4b) compose of hexapods at right angle. Four pods are in the same plane. The other two pods are at right angle to the four-pod structure. One pod is on the top, and the other is at the bottom. The CA and NA products (Figs 4c and 4d) compose of a number of cubes with different sizes. Their facets are very smooth like a mirror. The NC product (Fig 4e) shaped like fern. Each of its leaves slopes up to a point, and has two halves with the same in size and shape. The NT (Fig 4f) is similar to a magic square. It composes of four cubes in cubic cluster. The number of cubes containing along any row, column or diagonal has the same sum. Those for AA, CC and CT (Figs 5a-5c), they are rather round particles with nanometer in size. The crystalline degree can play the role in the morphologies as well.